

Gravo-thermal catastrophe in gravitational collapse and energy progenitor of Gamma-Ray Bursts

She-Sheng Xue

ICRANet Piazzale della Repubblica, 10 -65122, Pescara, Italy,
Physics Department, University of Rome La Sapienza,
P.le Aldo Moro 5, I-00185 Rome, Italy

E-mail: xue@icra.it and shesheng.xue@gmail.com

Abstract. We study the homologous collapse of stellar nuclear core, the virial theorem for hadron collisional relaxations, and photon productions from hadron collisions. We thus show the gravo-thermal dynamical process that transforms gravitational energy to photon energy. The process is energetically and entropically favourable. The total baryon number conservation, Euler equation for energy-momentum conservation and Poisson's equation for gravitational potential are adopted to describe homologous core collapses. The virial theorem determines the hadron collision energy gain from gravitational potential. The hadronic photon production rate determines the photon energy density. The time scales of macroscopic and microscopic processes are studied to verify approximations. As a result, we show the formation of opaque photon-pair spheres, whose total energy, size, temperature and number density, accounting for the main energetic features of Gamma-Ray Burst progenitors. We obtain the intrinsic correlations of these quantities. They depend only on the averaged thermal index of the stellar core. We discuss the possibility to confront them with observational data.

Contents

1	Introduction	2
2	Gravo-thermal catastrophe and virial theorem	3
3	Photon production from hadron collisions	4
4	Adiabatic process of gravitational collapse	7
4.1	Fundamental equations for gravitational collapse	7
4.2	Macroscopic and microscopic time scale hierarchy	8
5	Homologously collapsing stellar core	9
5.1	Basic gravitational length scale and sound velocity	9
5.2	Eigenvalue problem for homologous collapse configurations	10
6	Photon-pair sphere formation and properties	13
6.1	Photon-pair sphere temperature and energy density	13
6.2	Photon-pair sphere size and opacity	15
6.3	Total photon-pair sphere energy and number	16
7	Intrinsic correlations and connections with GRB sources	18
7.1	Photon-pair sphere characteristics	18
7.2	Universal scaling laws with only one index parameter	19
7.3	Possible connections to GRB observations	21
8	Thermodynamic of photon-pair sphere formation	22
8.1	Negative pressure and gravitational energy gain	22
8.2	Entropy increases in particle relaxation and production	23
9	Conclusion and remarks	24
10	Acknowledgment	26
11	Appendix: the time evolutions of homologous profiles	26

1 Introduction

Gamma-Ray Bursts (GRBs) are the most energetic and complex events in the Universe. One of the peculiar features is that the progenitors of these events release hard photons of tremendous energy $10^{49} \sim 10^{54}$ ergs in a few seconds. Since the last decades, great progress has been made for understanding the GRB natures [1–9]. However it still remains an open question what is the dominate dynamics of GRB progenitors, and many efforts have been made to find answers [7, 10–34]. It is no doubt that massive stellar gravitational potentials are great energy reservoirs, stellar collapse and coalescence must gain gravitational energies. How huge and invisible potential energies are converted to visible hard photon energies in just a few seconds, accounting for GRBs. Slowly hydrodynamical and kinematic processes are probably unlikely to make such rapid energy conversions. The most probable candidatures are electromagnetic and/or strong interacting processes. On the latter candidature, we mostly focus on this article.

In a self-gravitating system, Lynden-Bell and Wood [35, 36] pioneered the study of gravo-thermal catastrophe by using violent particle collisionless relaxation and virial theorem. The relevant dynamics and time scales in galactic and stellar systems have been discussed in the references, see for example [37–44]. We are inspired by the Lynden-Bell and Wood study, which shows the relaxation process that particles gain their mean kinetic heat energy from gravitational potential. On the other hand, we learn the hadron and quark-gluon photon productions by heavy-ion collisions. In the last decades, such photon productions have been intensively studied theoretically and experimentally in nuclear and particle physics [45–50]. This microscopic photon production process may have important applications in the arena of astrophysics and cosmology.

Suppose that hadrons inside compact stellar core gain gravitation energy by collisional relaxation, and hadron collisions produce photons. We study the gravo-thermal dynamics: how the gravitational core-collapse process converts the gravitational energy to photon energy and create a photon-pair sphere. To qualitatively show how the dynamics work, we adopt homologous core collapses [51] and discuss different time and length scales of macroscopic and microscopic processes. Using both analytical and numerical approaches for calculations, we show the formation of opaque and energetic photon-pair spheres, possibly explaining GRB progenitors.

We organise this article as follow. In Secs. 2 and 3, we present the discussions of gravo-thermal catastrophe, virial theorem, and photon productions from hadron collisions. We discuss the gravo-thermal dynamics by using homologically collapsing core in Secs. 4 and 5. In Secs. 6 and 7, we analyse photon-pair sphere properties and intrinsic correlations in connection with GRB progenitor features. Finally, we show that photon-pair sphere formation is energetically and entropically favourable in Sec. 8, and give conclusion and remarks in Sec. 9. The stellar core density is characterised by the nuclear saturation density $n_0 \approx 0.16 \text{ fm}^{-3} = 1.6 \times 10^{38} / \text{cm}^3$ or $\rho_0 = mn_0 \approx 2.4 \times 10^{35} \text{ ergs/cm}^3$, and $m \approx 1 \text{ GeV}$ is the typical baryon (neutron) mass. The light speed $c = 1$, Planck constant $\hbar = 1$ and Boltzmann constant $k = 1$ are used,

unless otherwise specified.

2 Gravo-thermal catastrophe and virial theorem

A stellar core is composed of nuclear matter, whose total mass M and baryon number $N = M/m$ of baryons of mass m ¹. This is a self-gravitating system. Its negative gravitational energy U and potential ϕ ,

$$U = \frac{1}{2} \int dx^3 \rho(x) \phi < 0, \quad \phi(x) = -G \int d^3x' \frac{\rho(x')}{|x - x'|}, \quad (2.1)$$

where G is the Newton constant. In the time-varying gravitational potential, via collisionless relaxation, baryons gain their mean kinetic energy from the gravitational energy. The baryon mean kinetic energy contributes to the core internal energy F , that in turn balances the self-gravitating potential energy. Such gravo-thermal catastrophe phenomenon of stellar cores is studied by considering violent relaxation [35] and equipartition theorem [36]. In these studies, they obtained the collisionless relaxation timescale $(3/4)(2\pi G\bar{\rho})$ of baryons in time-varying gravitational potential, in terms of the core mean density $\bar{\rho}$. The stellar core is assumed to be an isothermal core of temperature $T \ll m$ and internal “heat” energy $F = \frac{3}{2}TN \ll mN$. Moreover, they considered the isothermal core as an equilibrium or equipartition system. Therefore, the virial theorem of Clausius can be applied

$$2F + U = 3PV, \quad (2.2)$$

where V is the core volume and P is the external pressure, acting on the core surface.

These studies show that the baryon collisionless relaxation process in gravitational potential and external pressure leads to two consequences. (i) The gravitational energy is converted to the internal heat energy of baryon gas. (ii) The balance between gravitational dynamics and thermodynamics is established, and the virial theorem (2.2) is applicable. The second point is correct, provided the time scales of relaxation processes is much smaller than that of macroscopic gravitational and hydrodynamical processes.

For the reasons given in the next paragraph, we generalise these discussions from an entire stellar core to a small fluid element of volume dV inside the stellar core. The virial theorem (2.2) can be given by

$$2dF + dU = 3pdV, \quad dF = (3/2)T(\rho/m)dV, \quad dU = (1/2)\rho\phi dV, \quad (2.3)$$

and $dF \ll \rho dV$, i.e., $T \ll m$. Associating to each fluid element ρdV , the baryon temperature T characterises the mean kinetic energy of baryon motions and collisions. We approximately describe the internal pressure p by the equation of state (EoS)

$$p = \kappa\rho^\gamma, \quad (2.4)$$

¹By the term *baryons*, we indicate nucleons, nuclei, hadrons, quark-gluon plasma that carry baryon numbers.

with two parameters: mean thermal index γ and coefficient κ . The latter relates to the maximal value of core centre density ρ_c . Here we have to mention that the EoS (2.4) is adopted for this simple model and preliminary study. Because of large core density and possible phase transition, more complex types of EoS are expected, for example, γ and κ are not constants in space and time.

We will consider compact stellar cores of nuclear density so that equipartition or equilibrium should be achieved by the relaxation processes of baryon-baryon collisions. Unlike the virial theorem (2.2) based on collisionless relaxation, the virial theorem (2.3) mainly bases on collisional relaxation. The collisional relaxation timescale can be estimated as

$$\tau_{\text{relax}} = (\sigma_n v n)^{-1} \approx 5.21 \times 10^{-3} (n_0/n) (T/m)^{1/2} T^{-1} < T^{-1}, \quad (2.5)$$

where $n = \rho/m$ (v) is the baryon number density (mean velocity), $\sigma_n \approx 1/m_\pi^2$ is the typical cross-section of baryon-baryon collisions, and averaged collision energy (baryon temperature) $T = (1/2)mv^2 \ll mc^2$. The baryon collisional relaxation time scale τ_{relax} (2.5) is smaller than the time scales (T^{-1}) of baryon kinetic motion and collisionless relaxation². Therefore, a *local* equilibrium or equipartition state can be established. Thus, the *local* virial theorem (2.3) is applicable. As a consequence, the baryon temperature T is determined by

$$\begin{aligned} 3T/m &\approx 3v_s^2(1/\gamma) - (1/2)\phi, \\ v_s^2 &= \partial p / \partial \rho = \gamma p / \rho \end{aligned} \quad (2.6)$$

where v_s is the sound velocity. For an isothermal core, integrating Eq. (2.3) over the core volume $\int dV$, one obtains the virial theorem (2.2), using $\int p dV = PV$.

3 Photon production from hadron collisions

Through baryon-baryon collisions, baryons gain their mean kinetic (heat) energy from the gravitational potential of self-gravitating cores. The mean baryon collision energy is characterised by the baryon temperature T (2.6). Besides, the baryon-baryon collisions produce photons and pairs of light charged leptons and quarks, As a result, baryons' mean kinetic heat energy is converted to the energy of photons, and pairs of other light charged leptons and quarks.

From the studies of heavy-ion collisions, see for example references [45–50], we learn the hadron productions of photons in the heavy-ion collision. References [46, 47] show high-energy photons produced from quark-gluon plasma versus hot hadronic gas. The photon production rates of the quark-gluon plasma and the hadron gas are approximately the same in the energy range of a few hundred MeV. The transition from hadron matter to quark-gluon plasma (QGP) occurs at a temperature of about 200 MeV. In this energy range, quarks and gluons are deconfined in colourless particles,

²In Eq. (2.5), for $T \sim 10^2$ MeV and $n \sim n_0$, the baryon kinetic motion time scale $T^{-1} \sim 10^{-23}$ seconds, and the baryon collisional relaxation time scale (2.5) $\tau_{\text{relax}} \sim 10^{-26}$ seconds.

and become the pertinent degrees of freedom of the system. Given the temperature T of hadron gas (or quark gluon plasma) collisions, the photon production rate $R_\gamma = dN_\gamma/dtdV$ per volume is [45]

$$\frac{dR_\gamma}{d^3\vec{q}} = q_0^{-1} \frac{2\alpha\alpha_s}{3} T^2 e^{-q_0/T} \ln\left(1 + \frac{2.9}{4\pi\alpha_s} \frac{q_0}{T}\right), \quad (3.1)$$

where QED and QCD fine structure constants $\alpha = 1/137$ and $\alpha_s \approx 0.5$.

Based on the hadronic photon production (3.1) in heavy-ion collisions, the production rates of the photon number and energy densities can be calculated as,

$$\frac{dn_\gamma}{dt} = \int d^3\vec{q} \frac{dR_\gamma}{d^3q}, \quad \text{and} \quad \frac{d\rho_\gamma}{dt} = \int d^3\vec{q} q_0 \frac{dR_\gamma}{d^3q}. \quad (3.2)$$

In addition to photons, we consider pairs of relativistic charged leptons or quarks are approximately massless, i.e., $q^2 = q_0^2 - \vec{q}^2 = 0$ at energy scale T of a few hundred MeV. Their chemical potentials are zero, due to lepton- or baryon-number conservation. Integrating over the phase space $d^3\vec{q} = 4\pi q^2 dq$ in Eq. (3.1), we obtain,

$$R_\gamma \approx \frac{4}{3} \frac{\alpha\alpha_s}{\pi} T^4 \ln\left(1 + \frac{2.9}{4\pi\alpha_s}\right). \quad (3.3)$$

Here we use the saddle point approximation $q_0 \approx T$ to arrive at a simple formula for astrophysical applications. The exponential suppression factor $e^{-q_0/T}$ (3.1) shows the dominant photon production at energy $q_0 \sim T$. On the other hand, the Heisenberg uncertainty relation in thermal particle productions yields $q_0\tau \sim 1$. This implies that the thermal photon production time scale $\tau_{\text{prod}} \sim q_0^{-1} \sim T^{-1}$. Therefore, the photon number and energy densities (3.2) can be approximately estimated as,

$$n_\gamma \approx \frac{4}{3} \frac{\alpha\alpha_s}{\pi} T^3 \ln\left(1 + \frac{2.9}{4\pi\alpha_s}\right), \quad (3.4)$$

$$\rho_\gamma \approx \frac{8}{3} \frac{\alpha\alpha_s}{\pi} T^4 \ln\left(1 + \frac{2.9}{4\pi\alpha_s}\right). \quad (3.5)$$

We thus consistently define the production time scale

$$\tau_{\text{prod}} \equiv n_\gamma/R_\gamma \approx T^{-1} > \tau_{\text{relax}}. \quad (3.6)$$

These are qualitative properties of photons produced by heavy-ion collisions at baryon temperature T .

The photon productions by baryon-baryon collisions in an isothermal baryon core of temperature T (2.6) are inevitable. The necessary condition is that photons are massless, and no energy gap needs to overcome in their thermal production. Other relativistic charged lepton or quark pairs are approximately massless for temperature being much larger than their masses ($T \gg m_{\ell,q}$). The sufficient condition on the other hand is that the photon production time scale τ_{prod} (3.6) should be larger than the

relaxation time scale τ_{relax} (2.5). This is indeed the case $\tau_{\text{prod}} > \tau_{\text{relax}}$. The gravothermal catastrophe produces not only massive baryons' heat energy $(3/2)T(\rho/m)dV$ (2.3), but also relativistic particles' energy $\rho_\gamma dV$ (3.5).

For the baryon temperature $T \sim \mathcal{O}(10^2)$ MeV, the photon density n_γ (3.5) is so large that relativistic particles are opaqued and thermalized by collisions among themselves. The photon thermalization time scale, which is the mean-free path divided by the speed of light c , can be estimated by

$$\tau_{\text{therm}} = (\sigma_\gamma c n_\gamma)^{-1} \approx \frac{3.23 \times 10^6}{[\ln(2T_\gamma/m_e)]} \left(\frac{m_e T_\gamma}{T^2} \right) \frac{1}{T} \gg \tau_{\text{prod}}. \quad (3.7)$$

Here we use the Thomson cross section $\sigma_\gamma \approx \sigma_T(3/8)(m_e/T_\gamma) \ln(2T_\gamma/m_e)$ and $\sigma_T = (8\pi/3)\alpha^2/m^2$. The photon temperature T_γ represents the mean energy of photon collisions. The mean temperature T_γ of thermalized photons can be estimated by equating photon thermal energy density to Eq. (3.5)

$$\frac{\pi^2}{15} T_\gamma^4 \approx \rho_\gamma, \quad \Rightarrow \quad T_\gamma \approx 0.21T. \quad (3.8)$$

It shows that the photon temperature T_γ is the same order of the baryon temperature T . Inequality $\tau_{\text{therm}} \gg \tau_{\text{prod}}$ (3.7) implies that many photons are produced by baryon collisions before they are thermalised through their electromagnetic interactions. We further note that the viscous hydrodynamical evolutions of photons start at thermalisation time τ_{therm} [45, 52].

Moreover photons produced from baryon-baryon collisions electromagnetically are coupled to pairs of charged leptons (quarks) and anti-leptons (-quarks). Among these charged particle pairs, we particularly consider pairs of electrons and positrons, since their mass (MeV) is smaller than the photon characteristic energy $\sim T > \text{MeV}$ (2.6). Therefore the forth and back processes $\gamma + \gamma \leftrightarrow e^+ + e^-$ of electron and positron pair production and annihilation are kinematically possible. The cross section $\sigma_{\gamma\gamma \leftrightarrow e^+e^-}$ is of the order of the Thomson cross section σ_γ in Eq. (3.8), and the corresponding mean-free length $\sim (\sigma_{\gamma\gamma \leftrightarrow e^+e^-} n_\gamma)^{-1}$ is very small. This indicates that via processes $\gamma + \gamma \leftrightarrow e^+ + e^-$, photons and electron-positron pairs participate thermalisation or thermal equipartition in particle energy and number. In addition, electron-positron pairs can be produced by photons interacting with viral photons γ^* of classical external magnetic fields [53, 54]. Since the electron and positron pairs are relativistic at the energy scale under consideration, the degree freedoms of photon polarisation and electron-positron pair are the same, their thermal equipartition results in the particle energy densities $\rho_{e^+e^-} \approx \rho_\gamma$ and number densities $n_{e^+e^-} \approx n_\gamma$, conserving the total lepton number. Thus, a half of photons produced from baryon-baryon collisions converts to electron-positron pairs. Equation (3.8) becomes $(\pi^2/15)(T_\gamma^4 + T_{e^+e^-}^4) \approx \rho_\gamma$, where $T_\gamma \approx T_{e^+e^-}$. The same discussions can be applied to the inclusion of the lightest u and d quarks if the mean photon energy can excite them to participate in the thermalisation. As a result, these processes lead to an electrically neutral, deeply opaque and thermalised plasma (fluid) of photons and electron-positron pairs.

To end this section, it is worthwhile to have a brief discussion on other possibilities of photon productions from baryon-baryon collisions. We point out that the hadronic photon production (3.1) or (3.2) is proportional to $\alpha\alpha_s$. The strong QCD coupling constant α_s comes from the kinematic motion of charged quark-gluon matter (fluid) inside hadrons, which is predominately governed by the shorted ranged QCD dynamics. Whereas, the QED coupling constant α come from the charged quark-gluon matter coupling to photons, and producing photons via its QCD govern kinematic motion. It is conceivable that the kinematic motions of charged baryonic matter are partially governed by the long-ranged QED dynamics, and the photon production proceeds via QED processes like thermal bremsstrahlung, double Compton scattering, and Comptonized cyclotron/synchrotron in the presence of fluctuating electromagnetic fields in microscopic length scales and/or classical magnetic fields in macroscopic length scales. In this case, the photon production rates should be proportional to at least $\alpha\alpha$, which is smaller than $\alpha\alpha_s$. The reason for $\alpha\alpha$ is that both charged baryonic particle motions and radiations are attributed to the QED dynamics. These preliminary and qualitative discussions imply that the QCD hadronic photon-production rate (3.1) or (3.2) should be the leading order contribution, while the contributions from the QED photon-production processes should be the next leading order. Detailed and quantitative calculations should be possibly performed by simulations in heavy-ion collision physics. Nevertheless, the contributions from QED photon-production processes further increase the photon-production efficiency in baryon-baryon collisions. As a consequence, the total number density of produced photons should be larger than the one (3.4) from the QCD process. These QED processes are in favour of increasing the energy and number densities of thermalised plasma (fluid) of photons and electron-positron pairs, which we discussed above.

4 Adiabatic process of gravitational collapse

We now turn to study the gravo-thermal dynamics. How gravitational collapses convert the gravitational potential energy to the photon sphere energy via baryon collisional relaxation in gravitational potential, and baryon-baryon collisions for photon productions. The problems are that gravitational collapse is a dynamical avalanche process instead of a stationary process for which we discuss the virial theorem for particle collisionless relaxation in Sec. 2. Besides, baryon collisional relaxation and photon production are dynamical back reaction processes, as aforementioned. In practice, dealing with such a complex system, it is rather difficult for both analytical and numerical approaches to analyse all dynamics without any approximation. To make appropriate approximations, we need to understand what is dominant physical process and variation in given relevant length and time scales.

4.1 Fundamental equations for gravitational collapse

Following the approach to homologously gravitational collapsing [51], we adopt in Newtonian approximation the continuity equation for total baryon number conservation,

Euler equation for energy-momentum conservation and Poisson’s equation for gravitational potential ϕ ,

$$\frac{\partial \rho}{\partial t} + \nabla \cdot (\rho \mathbf{u}) = 0, \quad (4.1)$$

$$\left(\frac{\partial \rho}{\partial t}\right) + \nabla \cdot \left(\frac{1}{2} |\mathbf{u}|^2\right) + (\nabla \times \mathbf{u}) \times \mathbf{u} + \nabla h + \nabla \phi = 0, \quad (4.2)$$

$$\nabla^2 \phi - 4\pi G \rho = 0. \quad (4.3)$$

Here, \mathbf{u} is the baryon fluid velocity. Equation of State (2.4) yields the baryon heat function $h = H/\rho$ (H for Enthalpy)

$$\nabla h = \nabla p/\rho; \quad h = \int \nabla p/\rho = \frac{\kappa \gamma}{\gamma - 1} \rho^{\gamma-1}. \quad (4.4)$$

The gradient of heat function gives a thermal force against gravity. If the baryon fluid flow is vorticity free, the velocity can be obtained from a stream function $\mathbf{u} = \nabla v$ up to a constant. The Euler equation (4.2) becomes

$$\frac{\partial v}{\partial t} + \frac{1}{2} |\nabla v|^2 + h + \phi = 0. \quad (4.5)$$

In the following, we present the solution for arbitrary γ value, generalising the $\gamma = 4/3$ solution [51]. Note that for $\gamma < 4/3$, self-gravitating cores become dynamically unstable, and undergo gravitationally homologous collapses, see for example Refs. [55–57].

4.2 Macroscopic and microscopic time scale hierarchy

Self-gravitating core collapse processes have the time scale $\tau_{\text{grav}} = |\mathbf{R}|/|\dot{\mathbf{R}}|$, and $|\mathbf{R}|$ is the core radius. The notation τ_{grav} represents also the time scale $\sim |\mathbf{R}|/v_s$ of other hydrodynamical processes, where v_s is the sound velocity. As will be shown in next section 5, the τ_{grav} is a macroscopic time scale. It is much larger than the microscopic process time scales of baryon collisional relaxation τ_{relax} (2.5), photon production τ_{prod} (3.6) and thermalization τ_{therm} (3.7),

$$\tau_{\text{grav}} \gg \tau_{\text{therm}} > \tau_{\text{prod}} > \tau_{\text{relax}}. \quad (4.6)$$

This time scale hierarchy means that (i) these microscopic processes occur not only “instantaneously”, but also “locally” ($\ell_{\text{micro}} \approx c\tau_{\text{micro}} \ll |\mathbf{R}|$), comparing with gravitational collapsing and hydrodynamical process; (ii) there is no causal correlation among the concurrence of these microscopic processes at different space-time points in macroscopic scales. In other words, the vast difference in microscopic and macroscopic time scales implies that gravitational collapse can be considered as a very slowly *adiabatic* process, comparing with these rapid and local microscopic processes. Therefore, we regard that these microscopic processes can be approximately analysed, as if self-gravitating cores were static. Namely, in a gravitational collapse process, we can

approximately adopt the results of baryon temperature T (2.6) and photon temperature T_γ (3.8), as well as photon production number and energy densities (3.4,3.5), obtained in previously sections. It is what we call the *adiabatic* approximation.

Moreover, the shorter time scale process proceeds several times and has been well established in the smooth varying period of longer time scale processes. But the inverse is not correct. The time scale hierarchy (4.6) shows that the most rapidly established microscopic process is the baryon collisional relaxation (2.6). The photon production process (3.6) is less rapid. The photon thermalisation process (3.7) is the slowest one. These microscopic processes are well established within the smooth varying periods of gravitational collapse and hydrodynamical processes. This time sequence (4.6) provides a necessary condition for the gravo-thermal dynamics. Namely, from gravitational potential, baryons gain heat energy via their collisional relaxations (2.3). Via hadronic photon productions, baryons convert their heat energy to photon energy (3.3), which are then thermalised (3.7).

A priori, we give the reasons why such an *adiabatic* approximation can be adopted to study microscopic dynamics in gravitational collapsing and hydrodynamic processes. However, its self-consistency has to be verified *a posteriori*. It follows the same reasons, discussed in the pioneer works [58, 59]. There it is stated that the gravitational evolution time scale due to stellar evaporation and consumption is longer than the core relaxation time scale, the core will maintain an approximate isothermal core profile (2.2) and will evolve homologously.

5 Homologously collapsing stellar core

5.1 Basic gravitational length scale and sound velocity

We consider only the case of spherically symmetric stellar cores. The core radial coordinate is rescaled from (dimensioned) \mathbf{R} to (dimensionless) $\mathbf{r} = \mathbf{R}/a(t)$. The time dependent length scale function $a(t)$ is defined as

$$a(t) = (\gamma p_c / \rho_c)^{1/2} / (\gamma \pi G \rho_c)^{1/2} = \rho_c^{\frac{\gamma}{2}-1} \left(\frac{\kappa}{\pi G} \right)^{1/2}, \quad (5.1)$$

where the subscript or superscript c indicates the values at core center $\mathbf{R} = 0$ or $\mathbf{r} = 0$. The baryon density is rewritten as

$$\rho = \rho_c f^3, \quad \rho_c = \left(\frac{\kappa}{\pi G} \right)^{\frac{1}{2-\gamma}} a^{\frac{2}{\gamma-2}}, \quad (5.2)$$

where the core centre density $\rho_c = \rho_c(t)$ is a function of time, and homologous profile $f = f(r)$ is a function of dimensionless radius r only. The scale function $a(t)$ decreases and centre density $\rho_c(t)$ increases as gravitational collapse goes on. The gravitational potential ϕ is re-expressed

$$\phi = \left(\frac{\gamma p_c}{\rho_c} \right) \psi = (v_s^c)^2 \psi = \gamma \kappa \rho_c^{\gamma-1} \psi, \quad (5.3)$$

in terms of another homologous function ψ and the sound velocity

$$v_s^2 = \gamma p / \rho = (v_s^c)^2 f^{3(\gamma-1)}; \quad (v_s^c)^2 \equiv \gamma p_c / \rho_c = \gamma \kappa \rho_c^{\gamma-1}. \quad (5.4)$$

The sound velocity at core center $(v_s^c)^2 = \gamma p_c / \rho_c$ increases as the centre density ρ_c increases and scale function $a(t)$ decreases. The maximal sound velocity $(v_s^c)^2 = \gamma \kappa \rho_c^{\gamma-1} \leq 1/3$ [60] leads to the minimal scale length a_{\min} and maximal center density ρ_c^{\max}

$$a_{\min} = (3\gamma)^{\frac{2-\gamma}{2(\gamma-1)}} \left(\frac{\kappa^{\frac{1}{\gamma-1}}}{\pi G} \right)^{1/2}, \quad \rho_c^{\max} = (3\gamma \kappa)^{-\frac{1}{\gamma-1}}. \quad (5.5)$$

The sound velocity and baryon density can be expressed as

$$\rho_c = \rho_c^{\max} \left(\frac{a}{a_{\min}} \right)^{-\frac{2}{2-\gamma}}; \quad (v_s^c)^2 = \frac{1}{3} \left(\frac{a}{a_{\min}} \right)^{-2\frac{\gamma-1}{2-\gamma}} = \frac{1}{3} \left(\frac{\rho_c}{\rho_c^{\max}} \right)^{\gamma-1}. \quad (5.6)$$

These relates three functions $a(t)$, $(v_s^c)^2$ and ρ_c at the core centre. We will use the centre density ρ_c as the primal variable. The maximal core centre density ρ_c^{\max} (5.5) is about $5 \sim 8$ times the nuclear saturation energy density ρ_0 . To illustrate numerical results in this article we will adopt $\rho_c^{\max} = 10\rho_0$. Thus, the coefficient κ of EoS (2.4) is constrained. The only one parameter left is the averaged thermal index γ in EoS (2.4).

To present physical results and their relevance, we define the basic gravitational length in homologous collapse:

$$a_{\min} = 3.06 \times 10^5 (3\gamma)^{-1/2} \left(\frac{\rho_c^{\max}}{\rho_0} \right)^{-1/2} (\text{cm}). \quad (5.7)$$

The minimal scale length a_{\min} , ‘‘sound horizon’’, comes from Eq. (5.5). The scale a_{\min} gives the macroscopic length scale that we discussed in the time scale hierarchy (4.6).

5.2 Eigenvalue problem for homologous collapse configurations

Setting $\mathbf{u} = \dot{a}\mathbf{r}$ or $v = (1/2)a\dot{a}r^2$ [51], we reduce the continuity equation (4.1) to the trivial relation $\dot{f} = 0$ which states that the homologous profile f and density profile f^3 (5.2) do not evolve in time. Euler’s equation (4.5) is separable in spatial \mathbf{r} and temporal t variables,

$$\psi = \frac{1}{\gamma-1} \left(\frac{\lambda}{6} r^2 - f^{3(\gamma-1)} \right), \quad (5.8)$$

$$a^{\frac{\gamma}{2-\gamma}} \ddot{a} = -\frac{\lambda}{6} \frac{2\gamma}{\gamma-1} \left(\frac{\kappa^{\frac{1}{\gamma-1}}}{\pi G} \right)^{\frac{\gamma-1}{2-\gamma}}, \quad (5.9)$$

and λ is the eigenvalue. Via Eqs. (5.3) and (5.8), Poisson’s equation (4.3) yields the nonlinear eigenvalue equation for the homologous profile $f(r)$,

$$\frac{1}{r^2} \frac{d}{dr} \left(r^2 \frac{df^{3(\gamma-1)}}{dr} \right) + \frac{4(\gamma-1)}{\gamma} f^3 = \lambda, \quad (5.10)$$

and the boundary conditions are $f'(0) = 0$ and $f(0) = 1$.

The theoretical scheme turns out to be an eigenvalue problem. All physical solutions of eigenvalues (γ, λ_m) and $1 < \gamma < 4/3$ have to be numerically found, consistently with physical conditions and observations. Using numerical approach (mathematics), we first reproduce the $\gamma = 4/3$ solution [51], as a check of numerical algorithm. Furthermore, as shown in the left of Fig. 1, we find three physical solutions of homologous density profile f^3 corresponding to the selected eigenvalues (γ, λ_m) :

$$\textit{Orange} (1.24, 1.0 \times 10^{-4}); \textit{Blue} (1.23, 8 \times 10^{-5}); \textit{Green} (1.225, 8 \times 10^{-6}), \quad (5.11)$$

for which the homologous profile $f(r)$ becomes tangent to $f = 0$ at the outer radius r_s , namely $f'(r_s) \approx 0$. The corresponding outer radius r_s are:

$$\textit{Orange} (r_s \approx 23); \textit{Blue} (r_s \approx 36); \textit{Green} (r_s \approx 34), \quad (5.12)$$

corresponding to three cases of eigenvalues (γ, λ_m) (5.11). In this article, we illustrate physical results by using three colour lines (*orange, blue, green*), representing typically selected eigenvalues (5.11). The shadow in between these colour lines indicates other possible physical solutions.

These limiting eigenvalues λ_m (5.11) for $f'(r_s) \approx 0$ are reached when the core surface at r_s (5.12) is in free fall, see discussions in Ref. [51]. Using Eq. (5.10) and outer boundary condition $f'(r_s) \approx 0$, the mean core density $\bar{\rho}$ is obtained in terms of the core centre density

$$\bar{\rho} \equiv \frac{M}{(4\pi r_s^3/3)} = \frac{\int_0^{r_s} 4\pi r^2 dr \rho}{(4\pi r_s^3/3)} = \frac{\gamma}{4(\gamma-1)} \lambda_m \rho_c. \quad (5.13)$$

The M is the total mass of the homologously collapsing core. Both the core mean density $\bar{\rho}$ and the core centre density ρ_c are functions of the time t .

Given the eigenvalue λ , the first and second time integrations of the temporal equation (5.9) give

$$\frac{1}{2} \dot{a}^2 = \frac{\lambda \gamma (2-\gamma)}{6 (\gamma-1)^2} \left(\frac{\kappa^{\frac{1}{\gamma-1}}}{\pi G} \right)^{\frac{\gamma-1}{2-\gamma}} a^{2\frac{1-\gamma}{2-\gamma}} + C, \quad (5.14)$$

$$\frac{a(t)}{a_{\min}} = \left\{ 1 + \left[\frac{\lambda \gamma}{3(2-\gamma)(\gamma-1)^2} \right]^{\frac{1}{2}} \left(\frac{t}{\tau_{\min}} \right) \right\}^{2-\gamma}. \quad (5.15)$$

The basic gravitational time scale in homologous collapse is:

$$\tau_{\min} \equiv \left(\frac{1}{\pi G \rho_c^{\max}} \right)^{1/2} = 1.02 \times 10^{-5} \left(\frac{\rho_c^{\max}}{\rho_0} \right)^{-1/2} (\text{sec}), \quad (5.16)$$

and $\tau_{\min} = (3\gamma)^{1/2} a_{\min}$. When the time approaches to the ending of homologous collapse, $t \rightarrow \tau_{\min}$, the scale function $a(t)$ approaches to the ‘‘sound horizon’’, $a(t) \rightarrow a_{\min}$, and core centre density approaches to its maximal value, $\rho(t) \rightarrow \rho_c^{\max}$ (5.5). As a comparison, the time scale τ_{\min} is larger than the free-fall time scale $\tau_{ff} = [3\pi/(32G\bar{\rho})]^{1/2}$

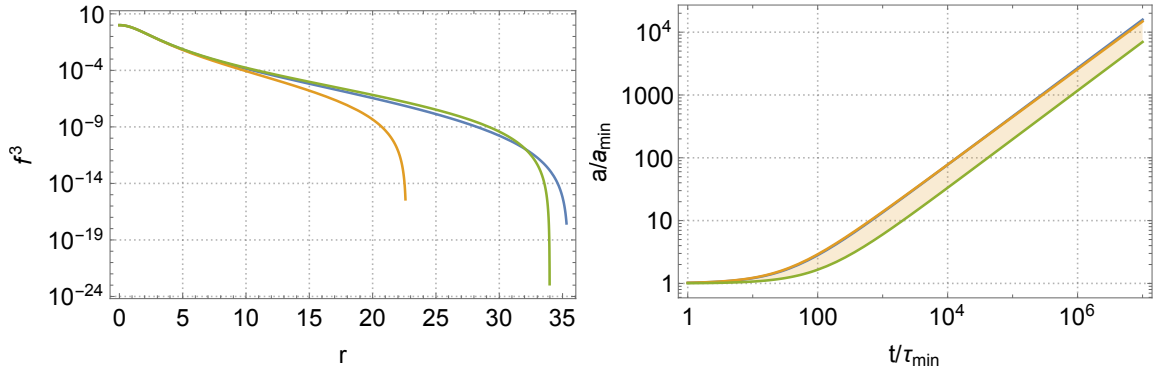


Figure 1. Colours on line for three eigenvalues (5.11). We show solutions to the eigenvalue problem (5.9) and (5.10). The homologous density profile f^3 is plotted (left) as a function of dimensionless radius $r = R/a$ (5.1). The density profile f^3 does not change in time, and it vanishes at the core outer radius $r = r_s$ (5.12). The scale function $a(t)/a_{\min}$ is plotted as in terms of t/τ_{\min} , using units a_{\min} (5.7) and τ_{\min} (5.16). Note that $t \sim 10^7 \tau_{\min} \sim \mathcal{O}(10)$ sec., depending on ρ_c^{\max} value.

for $\rho_c > \bar{\rho}$ (5.13). In fact the time scale τ_{\min} characterises the macroscopic time scale τ_{grav} that we discussed in the time scale hierarchy (4.6).

The constant of integration C in Eq. (5.14) determines the initial velocity of collapse. Its value has no great effect on the solution $a(t)$, when the scale function $a(t)$ approaches to the “sound horizon” a_{\min} (5.5). We put $C = 0$ and $\lambda > 0$ to obtain the second integration (5.15). The gravitational collapse process goes in the inverse time direction from the starting time $t > \tau_{\min}$ when $a = a(t)$ and $\rho_c = \rho_c(t)$, to the ending time τ_{\min} when $a \rightarrow a_{\min}$ and $\rho_c(\tau_{\min}) \rightarrow \rho_c^{\max}$. Namely, when the core starts homologous collapse at time t , its centre density is $\rho_c = \rho_c(t)$ and centre sound velocity $v_s^c = v_s^c(t)$, given the core mass M and radius r_s (5.13).

As results, the scale function $a(t)$ (5.15) is shown in the right of Fig. 1. The density ρ_c and sound velocity v_s^c at the core centre are shown in Fig. 2. These figures show the variations of scale function $a(t)$, centre density $\rho_c(t)$ and sound velocity $v_s^c(t)$ in homologous collapsing process from $t \sim 10$ seconds to $t \sim 10^{-5}$ seconds. The centre scale function $a(t)$ (5.1) and sound velocity $(v_s^c)^2(t)$ (5.4) are in terms of the centre density $\rho_c(t)$. All physical quantities are then functions of $\rho_c(t)$. While, at the time t when the core starts homologous collapse, the initial value $\rho_c(t)$ depends on the baryon core total mass M and its homologously collapsing radius r_s (5.13).

To illustrate the gravitational and thermal dynamics of homologous collapse, we also plot in Fig. 3 the positive heat function (4.4) and negative gravitational potential (5.3)

$$h = \frac{(v_s^c)^2}{\gamma - 1} f^{3(\gamma-1)}; \quad \phi = \frac{(v_s^c)^2}{\gamma - 1} \left(\frac{\lambda}{6} r^2 - f^{3(\gamma-1)} \right) \quad (5.17)$$

and their sum $h + \phi = \frac{(v_s^c)^2}{\gamma - 1} \frac{\lambda}{6} r^2$ in the Euler equation (4.5). The results depend on the thermal index γ in the equation of state (2.4) and the eigenvalue $\lambda > 0$. The latter relates to the material binding energy of baryon fluid per energy density ρ [51]. Indeed,

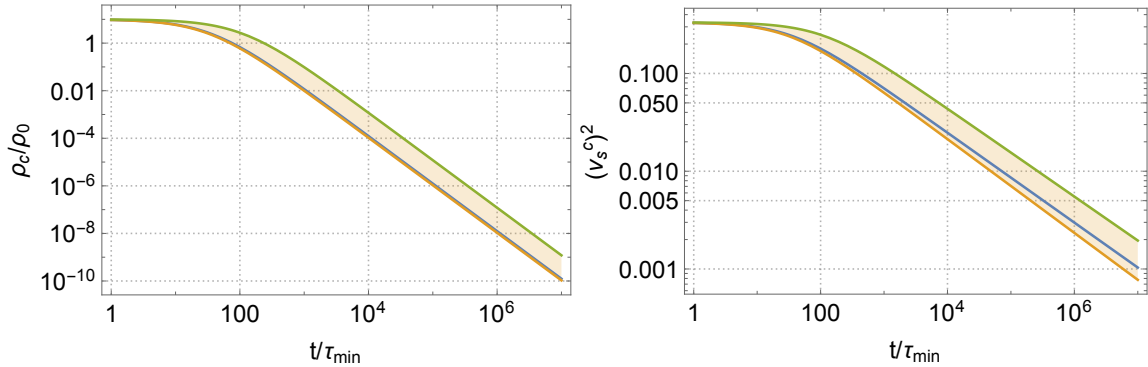


Figure 2. Colours on line for three eigenvalues (5.11). The core centre density ρ_c (left) and sound velocity $(v_s^c)^2$ (right) are plotted as functions of time in an homologous collapsing process. Their final values end up to $t = \tau_{\min}$ when $\rho_c = \rho_c^{\max} = 10\rho_0$ and $(v_s^c)^2 = 1/3$. Their initial values $\rho_c(t)$ and $(v_s^c)^2(t)$ depend on the initial time t , given the core mass M and radius r_s (5.13) and the validity of homologous collapse description. For instance, $t = 10^7 \tau_{\min} \sim \mathcal{O}(10)$ second, when $\rho_c = 10^{-(11\sim 10)} \rho_c^{\max} = 10^{-(10\sim 9)} \rho_0$ and $(v_s^c)^2 = (0.001 \sim 0.003)$.

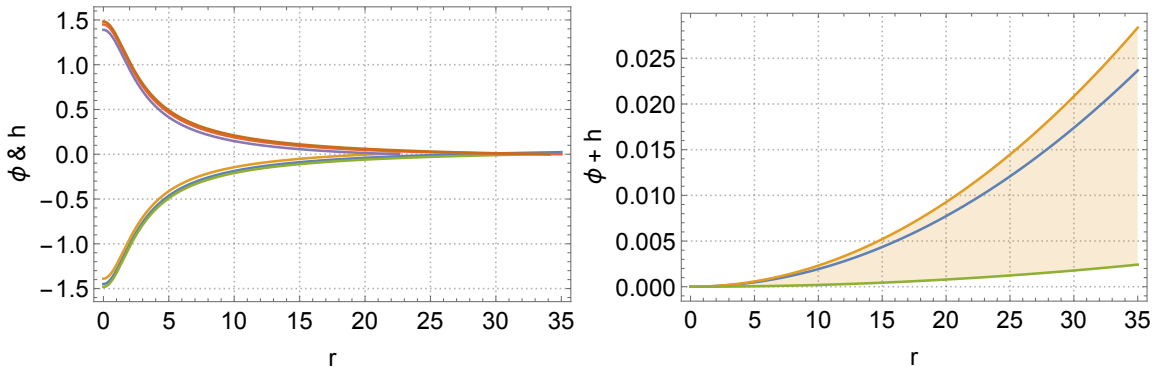


Figure 3. Colours on line for three eigenvalues (5.11). Using solutions (5.17) for maximal sound velocity $(v_s^c)^2 = 1/3$, the positive heat function h , negative gravitational potential ϕ (left) and their sum (right) are plotted as a function of dimensionless radius r . These homologous function (h, ϕ) profiles do not depend on the time t . However their amplitudes depend on the sound velocity $(v_s^c)^2(t)$. The time variations of these homologous profile amplitudes can be obtained by multiplying the sound velocity given by the right of Fig. 2.

our solutions (5.11) and (5.12) show that the binding energy λ_m value decreases, the outer boundary r_s becomes larger, i.e., the core is less bound, and the thermal index γ becomes smaller, i.e., the EoS (2.4) becomes soften.

6 Photon-pair sphere formation and properties

6.1 Photon-pair sphere temperature and energy density

On the basis of *adiabatic* approximation discussed below the time scale hierarchy (4.6), we use the “*local*” virial theorem (2.3) or (2.6) to obtain the baryon temperature T

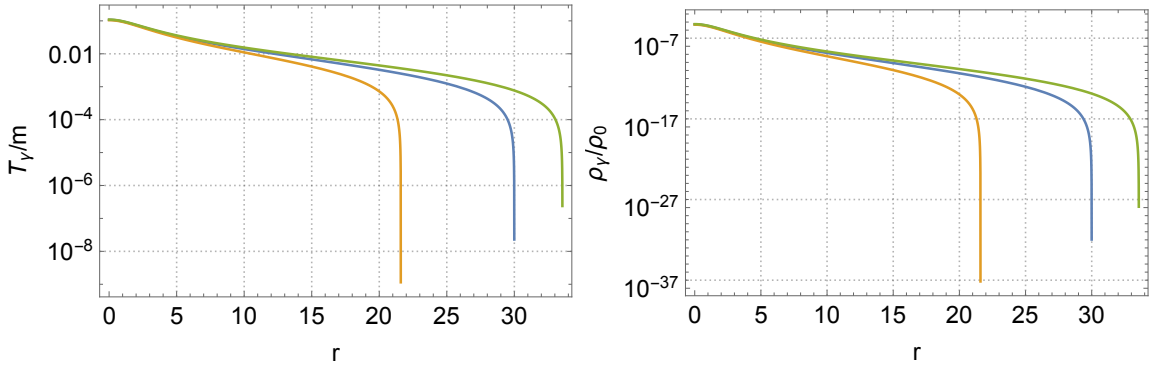


Figure 4. Colours on line for three eigenvalues (5.11). Using results (6.1) and (6.3) for maximal sound velocity $(v_s^c)^2 = 1/3$, we plot the homologous profiles of temperature T_γ/m (left) and energy density ρ_γ/ρ_0 (right) as a function of dimensionless radius r . Both profiles vanish at the photon-pair sphere radius r_γ (6.5), which is smaller than the core outer radius r_s (5.12), namely $r_\gamma < r_s$, see left of Fig. 1. Note that the typical hadron mass $m \approx 1$ GeV and nuclear saturation density $\rho_0 \approx 2.4 \times 10^{35}$ ergs/cm³. These homologous profiles do not depend on the time t . But their absolute values depend on time-dependent sound velocity $(v_s^c)^2(t)$, see Eqs. (6.1) and (6.3). The time evolutions of photon-pair sphere temperature $T_\gamma(r, t)/m$ (6.1) and energy density $\rho_\gamma(r, t)/\rho_0$ (6.3) are given in Fig. 7 in Appendix 11.

(2.6), then the photon-pair sphere temperature T_γ (3.8)

$$\frac{T_\gamma}{m} \approx 0.21(v_s^c)^2 \mathcal{T}(r), \quad \mathcal{T}(r) \equiv \frac{1}{6\gamma(\gamma-1)} \left[(7\gamma-6)f^{3(\gamma-1)} - \frac{\lambda}{6}\gamma r^2 \right]. \quad (6.1)$$

The time-dependent centre sound velocity $(v_s^c)^2$ comes from Eq. (5.4). The photon-pair sphere temperature T_γ reaches its maximum

$$\frac{T_\gamma^{\max}}{m} \approx 0.21(v_s^c)^2 \frac{(7\gamma-6)}{6\gamma(\gamma-1)}, \quad (6.2)$$

at photon-pair sphere centre $r = 0$. The photon-pair sphere temperature has no any lower limit, and it vanishes at the outer boundary $r = r_\gamma < r_s$, determined by $\mathcal{T}(r_\gamma) = 0$.

Furthermore, we use photon productions (3.4) and (3.5) by baryon collisions to approximately obtain the photon-pair sphere energy and number densities

$$\frac{\rho_\gamma}{\rho_0} \approx 1.29 \times \frac{4\alpha\alpha_s}{3\pi} \left(\frac{T_\gamma}{m} \right)^4 \ln \left(1 + \frac{2.9}{4\pi\alpha_s} \right), \quad (6.3)$$

$$\frac{n_\gamma}{n_0} \approx 6.16 \times \frac{4\alpha\alpha_s}{3\pi} \left(\frac{T_\gamma}{m} \right)^3 \ln \left(1 + \frac{2.9}{4\pi\alpha_s} \right). \quad (6.4)$$

In Fig. 4, we plot the photon-pair sphere temperature T_γ/m and energy density ρ_γ/ρ_0 for $(v_s^c)^2 = 1/3$. As a self-consistency check, we find that the baryon temperature T and photon temperature T_γ are much smaller than baryon mass ($T_\gamma \approx 0.21T \ll m$). The condition is fully filled for applying the virial theorem (2.3).

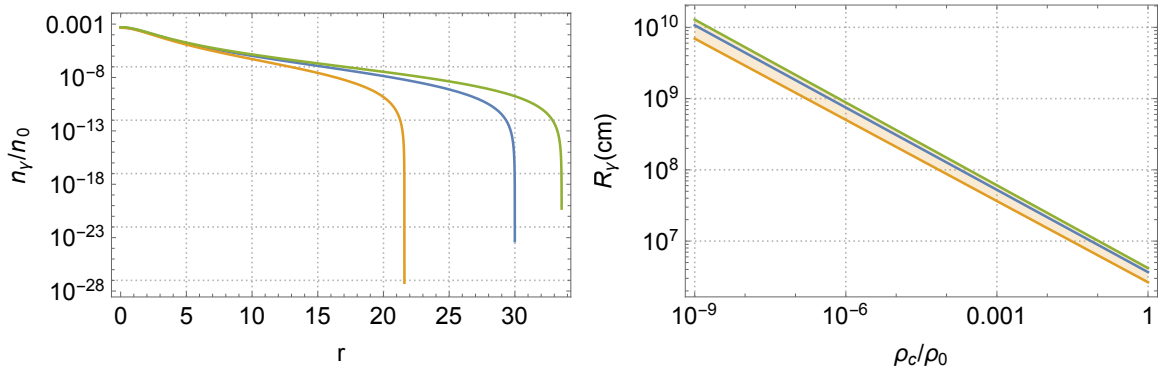


Figure 5. Colours on line for three eigenvalues (5.11). For maximal sound velocity $(v_s^c)^2 = 1/3$, we plot (left) the photon number density n_γ/n_0 (6.4) vanishes at outer boundary r_γ (6.5). The photon-pair sphere size $R_\gamma = ar_\gamma$ (6.8) (right) is plotted as a function of the initial core centre density $\rho_c(t)$ at the time t when core homologous collapse starts. The nuclear saturation density is $n_0 \approx 1.6 \times 10^{38}/\text{cm}^3$ or $\rho_0 \approx 2.4 \times 10^{35}\text{ergs}/\text{cm}^3$. The time evolution of photon-pair sphere number density $n_\gamma(r, t)/n_0$ (6.4) profile is given in Fig. 7 in Appendix 11.

In addition, the photon energy density ρ_γ (3.5) is much smaller than not only baryon mass-energy density ρ , but also baryon heat energy density $(3/2)T\rho/m$ (2.3). This justifies *a posteriori* that the photon-pair sphere energy density ρ_γ and heat function (thermal potential) $h_\gamma = \rho_\gamma + p_\gamma$ can be neglected in homologous collapse dynamics, studied in previous Sec. 5. Further discussions on the effective photon heat function will be presented in Sec. 8.

The “instant” and “locality” of microscopic processes discussed below the time hierarchy (4.6) are necessary conditions that, and reasons why photons produced can form an optic thick sphere or jet at macroscopic scales. Such trapped photons are in collective motions through density perturbations and/or other hydrodynamical processes of time scale $\sim |\mathbf{R}|/v_s$.

6.2 Photon-pair sphere size and opacity

As shown in Fig. 4, the photon-pair sphere temperature and energy density profiles vanish at dimensionless radius $r_\gamma < r_s$:

$$\text{Orange } (r_\gamma = 21.59); \text{ Blue } (r_\gamma = 30.00); \text{ Green } (r_\gamma = 33.56), \quad (6.5)$$

corresponding to three cases of eigenvalues (γ, λ_m) (5.11) and r_s (5.12). This determines the photon-pair sphere radial size $R_\gamma = a(t)r_\gamma$ (5.1). Using Eqs. (5.6), (5.7) and (5.15), we obtain

$$R_\gamma = 3.06 \times 10^5 (3\gamma)^{-1/2} r_\gamma \left(\frac{\rho_0}{\rho_c^{\max}} \right)^{\frac{\gamma-1}{2}} \left(\frac{\rho_0}{\rho_c} \right)^{\frac{2-\gamma}{2}} \text{ (cm)}, \quad (6.6)$$

which is plotted in Fig. 5 as a function of initial core centre density $\rho_c = \rho_c(t)$, when a homologous collapse initiates. This result shows that the photon-pair sphere radius

R_γ depends weakly on the eigenvalue $r_\gamma(\gamma, \lambda_m)$, which is independent of the time t . This behaviour is shown in some details by the homologous profiles given in Fig. 7 in Appendix 11. The photon-pair sphere radius R_γ decreases, as the initial core centre density $\rho_c(t)$ increases. The reason will be given below when we discuss the total photon-pair sphere energy and number.

Moreover, we show in Fig. 5 the photon-pair sphere number density n_γ (6.4) and photon-pair sphere size $R_\gamma = ar_\gamma$ (6.6). The results show that the photon number density n_γ is in the range of $(10^{37} \sim 10^{30})/\text{cm}^3$, and photon-pair sphere size R_γ is in the range of $(10^7 \sim 10^{10})$ cm. The photon-pair sphere is deeply opaque, since the photon mean-free path $\lambda_\gamma = (\sigma_\gamma n_\gamma)^{-1}$ is much smaller than the photon-pair sphere size R_γ , namely $\sigma_\gamma n_\gamma R_\gamma \gg 1$.

On the other hand, we find in Fig. 4 that the photon-pair sphere temperature T_γ can be well above the critical energy threshold $2m_e = 1.02$ MeV of electron-positron (e^+e^-) pair production. The photon-pair sphere energy density ρ_γ can be well above the critical energy density $\rho_e = m_e^4 = 5.93 \times 10^{-11} \rho_0$ of electron-positron pairs. This means that the photons are quickly thermalised to form an electro-position-photon plasma characterised by the thermalisation time scale τ_{therm} (3.7) [14, 17, 61], as briefly discussed in Sec. 2.

6.3 Total photon-pair sphere energy and number

The total relativistic particle energy E_γ and number N_γ of photon-pair sphere can be obtained by numerically integrating the energy density (6.3) and number density (6.4) over the photon-pair sphere volume $\int d^3R = a^3 \int 4\pi r^2 dr$. For comparison, we also compute the total baryon core mass $M = \int \rho d^3R = \rho_c a^3 F_0$ and number $N = M/m$, where $F_0 \equiv \int_0^{r_s} 4\pi r^2 dr f^3$. Defining coefficients $Y_n \equiv \int_0^{r_\gamma} 4\pi r^2 dr [\mathcal{T}(r)]^n$, we obtain

$$\frac{E_\gamma}{M} \approx 1.29 \times \left(\frac{1}{3}\right)^4 \frac{4\alpha\alpha_s}{3\pi} \ln\left(1 + \frac{2.9}{4\pi\alpha_s}\right) \frac{Y_4}{F_0} \left(\frac{\rho_c^{\text{max}}}{\rho_0}\right)^{4(1-\gamma)} \left(\frac{\rho_0}{\rho_c}\right)^{5-4\gamma} \quad (6.7)$$

$$\frac{N_\gamma}{N} \approx 6.16 \times \left(\frac{1}{3}\right)^3 \frac{4\alpha\alpha_s}{3\pi} \ln\left(1 + \frac{2.9}{4\pi\alpha_s}\right) \frac{Y_3}{F_0} \left(\frac{\rho_c^{\text{max}}}{\rho_0}\right)^{3(1-\gamma)} \left(\frac{\rho_0}{\rho_c}\right)^{4-3\gamma}. \quad (6.8)$$

We expressed them in terms of the core centre density $\rho_c = \rho_c(t)$ at the time t when the core starts to homologous collapse. Whereas, the time evolution of core centre density ρ_c can be found in Fig. 2 or Eq. (5.6).

Results (6.7), (6.7) and (6.8) show the photon-pair sphere size R_γ , energy E_γ and number N_γ depend on the initial core centre density ρ_c and the averaged thermal index γ . When the massive core starts to homologous collapse, the smaller initial value of the core centre density $\rho_c(t)$ is, the more extend core mass density profile $\rho(r, t)$ is, provided total core mass M and baryon number N fixed and conserved. As a consequence, the more gravitational energy can be gained in collapse and converted to the photon-pair sphere energy E_γ so that the photon-pair sphere size R_γ and number N_γ are larger as well. However, in contrast, these quantities are also power functions of the averaged thermal index γ , that represents the core repulsive reaction against gravitational collapse and energy gain. As shown in Fig. 6, we notice that for a large

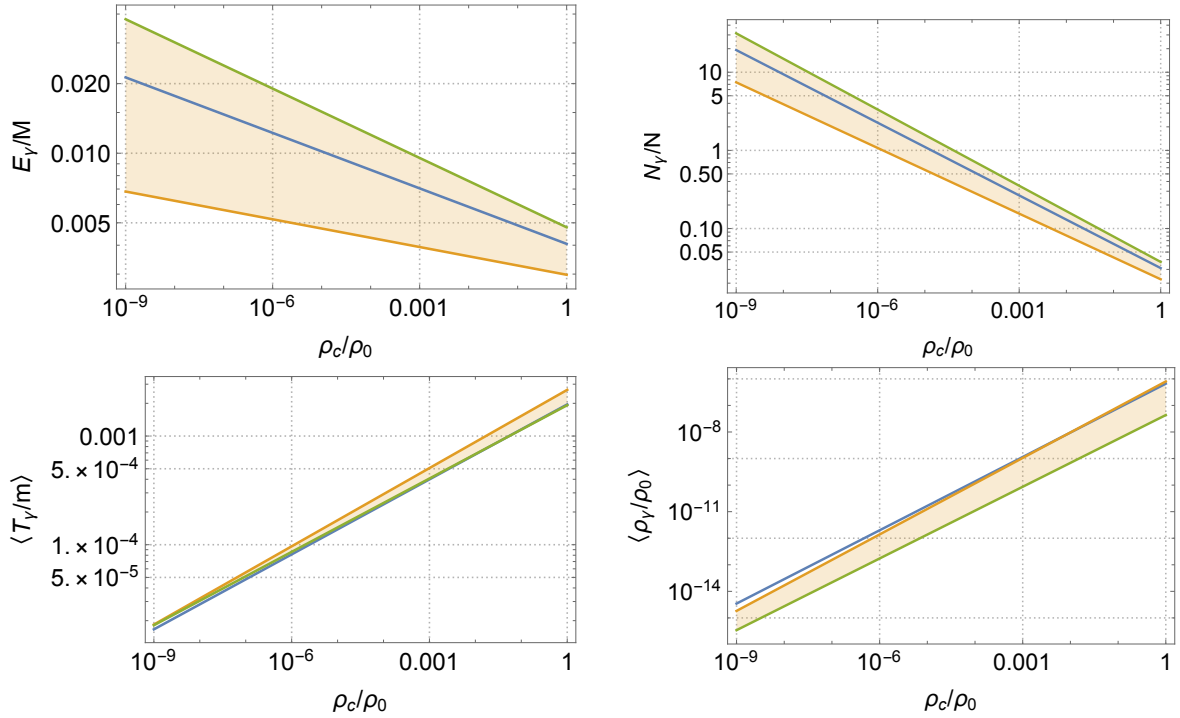


Figure 6. Colours on line for three eigenvalues (5.11). Top panel: the total photon sphere energy E_γ/M (6.7) (left) and number N_γ/N (6.8) (right); bottom panel: the mean photon-pair sphere temperature $\langle T_\gamma \rangle/m$ (6.9) (left) and energy density $\langle \rho_\gamma \rangle/\rho_0$ (6.10) (right), are plotted as a function of the initial core centre density ρ_c , when homologous collapse starts. The nuclear saturation density $\rho_0 \approx 2.4 \times 10^{35} \text{ergs/cm}^3$ and typical hadron mass $m \approx 1$ GeV. M and N are total mass and baryon number of the homologous collapsing core, $M_\odot \approx 1.8 \times 10^{54} \text{ergs}$ and $N_\odot \approx 1.2 \times 10^{57}$. The ratio $\rho_c(t)/\rho_0$ relates to the time t/τ_{min} when the collapse start, see Fig. 2.

variation of the core centre density ρ_c/ρ_0 , the total photon-pair sphere energy E_γ/M slowly varies within a order of magnitude. As an illustration, in Fig. 6, we make plots starting from the core centre density $\rho_c(t) \sim 10^{-9}\rho_0$ corresponds to the core collapsing time $t \approx 10^7\tau_{\text{min}} \sim 10$ sec., see Fig. 2. From these figures 1, 2, 5, and 6, people can find baryon core and photon-pair sphere properties, given an initial collapsing core density $\rho_c(t)/\rho_0$ and time t/τ_{min} , e.g., $\rho_c(t)/\rho_0 \sim 10^{-3}$ and time $t/\tau_{\text{min}} \sim 10^3$.

In addition, we define the mean photon-pair sphere temperature and energy density as averaged values of T_γ (6.1) and ρ_γ (6.3) over photon-pair sphere volume $(4\pi/3)r_s^3$,

$$\frac{\langle T_\gamma \rangle}{m} \equiv 0.21(v_s^c)^2 \frac{Y_1}{(4\pi/3)r_\gamma^3} = 0.21 \left(\frac{1}{3}\right) \frac{Y_1}{(4\pi/3)r_\gamma^3} \left(\frac{\rho_0}{\rho_c^{\text{max}}}\right)^{\gamma-1} \left(\frac{\rho_c}{\rho_0}\right)^{\gamma-1}, \quad (6.9)$$

$$\frac{\langle \rho_\gamma \rangle}{\rho_0} \equiv \frac{E_\gamma}{(4\pi/3)a^3 r_\gamma^3 \rho_0} = \left(\frac{E_\gamma \bar{\rho}}{M \rho_0}\right) \left(\frac{r_s}{r_\gamma}\right)^3 = \frac{\gamma \lambda_m}{4(\gamma-1)} \left(\frac{E_\gamma}{M}\right) \left(\frac{r_s}{r_\gamma}\right)^3 \left(\frac{\rho_c}{\rho_0}\right). \quad (6.10)$$

These represent the characteristic temperature and energy density of the photon-pair sphere. They are plotted in the bottom panel of Fig. 6 as functions of the initial core

centre density $\rho_c(t)$, when homologous collapse starts. Beside, the photon dimensionless energy $\nu/\langle T_\gamma \rangle$ and distribution function $F_\nu(\nu/\langle T_\gamma \rangle)$ in phase space are relativistic and cosmological redshift invariants resulting from the Liouville theorem (see e.g. [62]). The photon energy ν has a maximum (or peak energy) at $\nu_\gamma^{\max} \propto \langle T_\gamma \rangle$.

We close this section with the following emphases. Instead of photon-pair spheres, photon-pair jets are formed for angular momentum conservation in the cases of rotating stellar core collapse, two stellar cores merger, and the presence of strong magnetic fields. Such a photon-pair jet is in the direction along with the system axial symmetric axis. One can study a photon-pair jet by considering the centrifugal or magnetic potentials with gravitational potential ϕ in the local virial theorem (2.3). The physical quantities should be functions of radius r and azimuth angle θ , characterised by not only the initial core centre density $\rho_c(t)$, but also photon-pair jet collimation angle θ_{coll} determined by system angular momenta and magnetic fields.

7 Intrinsic correlations and connections with GRB sources

We have just shown the possible mechanism of how the vast gravitational energy converts to the huge energy of an opaqued photon-pair sphere energy in homologous core collapses. In the case that photon-pair sphere heat energy is much larger than its baryon loading, such an energetic photon-pair sphere/jet undergoes ultra-relativistically hydrodynamic outward expansion, and its temperature and radius thickness remains approximately T_γ and R_γ due to relativistic effects. At the transparency point, the photon-pair sphere becomes a photosphere. These were studied in the literature, and some details of using hydrodynamic equations and rate equation of back and forth process $\gamma + \gamma \leftrightarrow e^+ + e^-$ in general relativity framework can be found in Refs. [63–65]. During relativistic expansion, photon-pair sphere/jet proceeds “internal” energy dissipation processes, it sweeps and interacts with the circumburst media executing the “external” energy dissipation processes, accounting for GRB phenomena. Thus, the photon-pair sphere/jet kinematic motions (baryon loading and collimation), dynamical interactions (collisions, shocks and fluid dynamics) and energy dissipation mechanism (particle accelerations and radiation mechanisms) are important and have been modelled to account for the complex phenomena of GRB sources observed, see for example Refs. [1–8]. The opaqued photon-sphere formation is only the initial phase of GRB engines (progenitors). Therefore our present study is not in the position of directly explaining complex phenomena of GRB sources observed. Nevertheless, we examine photon-pair sphere properties and possible connections with GRB observations in this section.

7.1 Photon-pair sphere characteristics

The total core mass M , initial core centre density $\rho_c(t)$, and eigenvalue (γ, λ_m) uniquely represent different configurations of homologically collapsing core,

$$\{M, \rho_c(t), (\gamma, \lambda_m)\}. \quad (7.1)$$

The configuration determines the homologous core density profile $f^3(r)$, outer boundary radius r_s (5.12) and the photon sphere radius R_γ (6.5), see Eq. (5.13), as well as all other baryon core and photon-pair sphere quantities we have obtained. The various configurations (7.1) in fact correspond to different photon-pair spheres.

From the results presented in Fig. 6, we find the ranges of the total photon-pair sphere energy $E_\gamma \sim (10^{-2} \sim 10^{-4})M$ and number $N_\gamma \sim (1 \sim 10^{-3})N$, taking into account the centre sound velocity $(v_s^c)^2$ variation, see right of Fig. 2. These results are consistent with the total energy and entropy budgets. They are necessarily required to explain the cosmological origin of GRB phenomena observed. On the other hand, recall that the variation of gravitational energy $GM^2/(2R)$ is $M/4$ for a core-collapse from infinity $R = \infty$ to $R = 2GM$. It implies that the total photon-pair sphere energy E_γ is only a few per cent of maximally available gravitational energy $M/4$. The rest could be for core hydrodynamical and kinematic motion, as well as gravitational wave (non-spherical collapse) and other particles emissions. Such conversion from the available gravitational energy to the photon-pair sphere energy occurs in a couple of seconds. It means that the gravo-thermal dynamics is very efficient via hadron collisional relaxation and photon production in gravitational collapses.

Depending only on the averaged core thermal index $1 \lesssim \gamma \lesssim 4/3$, Figures 4, 5 and 6 represent the qualitative results and characteristic properties of the photon-pair sphere, namely the photon temperature T_γ , energy density ρ_γ and number density n_γ , as well as the photon-pair sphere size R_γ and opacity. These results show that the photon-pair sphere is deeply opaque, highly energetic and rather sizeable. Its temperature, size, energy and number densities are in the correct ranges, necessarily for the initial configurations of the opaque photon-pair sphere, i.e., *fireball or fireshell*, that subsequently undergoes various hydrodynamical and electromagnetic evolutions to explain GRB phenomena observed.

Notwithstanding, we show that the gravo-thermal dynamics can necessarily account for main energetic natures of GRB progenitor dynamics. In general, the realistic situations of gravitational collapse, baryon collisional relaxation and photon production are much more complicated. It is expected that the photon-pair sphere energy and number densities are reduced, the energy spectrum is softened, and the collapsing time is prolonged. Among others, the main reasons are that internal perturbation and/or shock waves are formed due to the baryon matter EoS (2.4) variations, phase transition and hydrodynamics, as well as the presence of macroscopic electromagnetic fields and thermal photon-pair sphere dynamics, even general relativistic effects. These are beyond the scopes of this article and subjects for future studies.

7.2 Universal scaling laws with only one index parameter

All physical quantities of photon-pair sphere are described in the rest frame anchored to the origin of homogeneously collapsing core. The photon-pair sphere size R_γ (6.6), total energy E_γ (6.7), mean temperature $\langle T_\gamma \rangle$ (6.9) and energy density $\langle \rho_\gamma \rangle$ (6.10) depend on the core centre density $\rho_c(t)$ (7.1) when homologous core collapse starts. Therefore they are intrinsically related each others via $\rho_c(t)$. Equation (6.9) gives $\langle T_\gamma \rangle \propto (\rho_c)^{\gamma-1}$, and Eq. (6.7) gives $E_\gamma \propto (\rho_\gamma/\rho_c) \propto \langle T_\gamma \rangle^4/\rho_c \propto \rho_c^{(4\gamma-5)}$. Recall that the initial core centre

density $\rho_c(t)$ values (7.1) represent different GRB sources. As a result, eliminating the dependence on $\rho_c(t)$, we qualitatively obtain the intrinsic correlation or universal scaling law between the photon-pair sphere total energy E_γ and characteristic energy scale (temperature) $\langle T_\gamma \rangle$

$$E_\gamma \propto \langle T_\gamma \rangle^\chi, \quad \chi = \frac{4\gamma - 5}{\gamma - 1} > 0. \quad (7.2)$$

This correlation (7.2) and those below are universal for all photon-pair spheres in the scenes that they are independent of the homologously collapsing core mass M and initial core centre density $\rho_c(t)$ in Eq. (7.1). Here the theoretical index χ depends on the averaged value of effective thermal index γ . The present theoretical model and EoS (2.4) are too simple and preliminary to quantitatively determine the averaged value of effective thermal index γ . Nevertheless, we find that $\gamma \sim \mathcal{O}(1)$ values are on the right spot to give $\chi \sim \mathcal{O}(1)$ in Eq. (7.2). We will treat $\chi \sim \mathcal{O}(1)$ as a unique parameter for all correlations discussed here.

From the viewpoint of total photon-pair sphere energy conservation, we can define the total photon-pair sphere luminosity

$$L_\gamma \equiv 4\pi c R_\gamma^2 \langle \rho_\gamma \rangle \propto \langle \rho_\gamma \rangle \rho_c^{-(2-\gamma)} \propto \rho_c^{5\gamma-6} \propto \langle T_\gamma \rangle^{(\chi+1)}. \quad (7.3)$$

This gives rise to the correlation of photon-pair sphere luminosity and temperature. The correlating index is not a new parameter, but $(\chi + 1)$ relating to the index χ in the correlation (7.2). The $E_\gamma - T_\gamma$ (7.2) and $L_\gamma - T_\gamma$ (7.3) correlations lead to $E_\gamma - L_\gamma$ correlation,

$$E_\gamma \propto L_\gamma^{\frac{\chi}{\chi+1}}. \quad (7.4)$$

With only one free parameter $\chi \sim \mathcal{O}(1)$, three correlations $E_\gamma - T_\gamma$ (7.2), $L_\gamma - T_\gamma$ (7.3) and $E_\gamma - L_\gamma$ (7.4) coherently reflect the energetic natures of gravo-thermal dynamics, which possibly explains GRB energetics.

Moreover, the photon-pair sphere size R_γ (6.6) represents the characteristic time scale $\tau_\gamma = R_\gamma/c$ of the photon-pair sphere. It should relate the temporal duration of GRBs. Equation (6.6) gives $R_\gamma \propto \rho_c^{-(2-\gamma)/2}$ dependence on the core centre density $\rho_c(t)$. Using the E_γ , T_γ and L_γ relations to the core center density $\rho_c(t)$, we obtain three anti-correlations $T_\gamma - \tau_\gamma$, $E_\gamma - \tau_\gamma$ and $L_\gamma - \tau_\gamma$:

$$\langle T_\gamma \rangle \propto \tau_\gamma^{-\delta} = \tau_\gamma^{-\frac{2}{3-\chi}}, \quad (7.5)$$

$$E_\gamma \propto \tau_\gamma^{-\chi\delta} = \tau_\gamma^{-\frac{2\chi}{3-\chi}}, \quad (7.6)$$

$$L_\gamma \propto \tau_\gamma^{-\delta(\chi+1)} = \tau_\gamma^{-\frac{2(\chi+1)}{3-\chi}}, \quad (7.7)$$

where

$$\delta \equiv 2\frac{\gamma-1}{2-\gamma} = \frac{2}{3-\chi} > 0. \quad (7.8)$$

These are consistent with correlations (7.2), (7.3) and (7.4), and indeed $E_\gamma \propto L_\gamma \tau_\gamma$ as it should be. Three anti-correlations $T_\gamma - \tau_\gamma$, $E_\gamma - \tau_\gamma$ and $L_\gamma - \tau_\gamma$ coherently reflect the time-scale natures of gravo-thermal dynamics for GRB energetics.

Via the sound velocity $(v_s^c)^2$ (5.6) at the core center, the maximal photon-pair sphere temperature $T_\gamma^{\max} \propto (\rho_c)^{\gamma-1}$ (6.2). Its dependence on the core center density ρ_c is in the same way as the mean temperature $\langle T_\gamma \rangle \propto (\rho_c)^{\gamma-1}$ (6.9), and $T_\gamma^{\max} \approx 6.87 \langle T_\gamma \rangle$. Therefore the correlations between T_γ^{\max} and other physical quantities can be obtained by substituting T_γ^{\max} for $\langle T_\gamma \rangle$ in Eqs. (7.2), (7.3) and (7.5). These could be of some interests. Because the maximal photon-pair sphere temperature T_γ^{\max} might be related to the high-energy threshold of GRB photons.

The theoretical correlations (7.2), (7.3) and (7.4), anti-correlations (7.5), (7.6) and (7.7) are not completely independent each other. However they base on only one free parameter $\chi \sim \mathcal{O}(1)$. They should receive corrections from the cosmological redshift z , $E_\gamma \rightarrow E_\gamma/(1+z)$, $\langle T_\gamma \rangle \rightarrow \langle T_\gamma \rangle/(1+z)$, $\tau_\gamma \rightarrow \tau_\gamma(1+z)$ and $L_\gamma \rightarrow L_\gamma$.

7.3 Possible connections to GRB observations

The theoretical correlation (7.2) seems to be the empirical Amati/Yonetoku relation $E_{\text{iso}} \propto E_p^2$ in GRBs [66, 67], if we identify the photon-pair sphere energy E_γ and mean energy $\langle T_\gamma \rangle$ to the observed total isotropic energy E_{iso} and peak energy E_p , or ν_γ^{\max} at which the maximum of photon energy spectrum νF_ν locates. However, we cannot simply make such identification for the reasons that the photon-pair sphere undergoes complex processes up to the transparency at which it becomes an observably relevant photosphere. One of reasons is that the peak energy E_p value sensitively depends on the photon-pair sphere baryon loading, see for example, Refs. [63, 64, 68, 69]. We attempt to give a general discussion on the possible connections between theoretical correlations (7.2-7.8) of different photon-pair spheres and observational correlations of different GRB sources.

The photon-pair spheres provide the necessary energy budgets for GRB events. Suppose that each photon-pair sphere created by a gravitational collapse process corresponds to a GRB event/source observed. As aforementioned at the beginning of the section, a photon-pair sphere (*initial state*) undergoes complex (*intermediate processes*) to a (*final state*) of GRB phenomena observed. The photon-pair sphere quantities T_γ , E_γ , L_γ and R_γ are not exactly the same as observed GRB event's mean energy, total energy, total luminosity, and time duration. Therefore, the correlations (7.2-7.8) cannot be directly examined by observed GRB events. However, photon-pair spheres' overall quantities ($T_\gamma, E_\gamma, L_\gamma, R_\gamma$) and basic relations (7.2-7.8) must imprint themselves in GRB data measured. Though the intermediate processes from a photon-pair sphere to an observed GRB source are complex, they are randomly different from one GRB source to other. Such randomness implies that the data of GRB events relevant to overall photon-pair sphere quantities should scatter around the basic relations (7.2-7.8) if these scaling relations truly reflect the universal natures of centre engines for GRB energetics. The more GRB events are taken into account, the more statistically confident level will be achieved on the validity of the basic relations (7.2-7.8) of photon-pair spheres. However, these are very general discussions. The relevant GRB phase

identification, spectrum and event selection, elaborate data analysis are required to give conclusions. These are subject to future studies. If these theoretical correlations and scaling laws are correct and verified, GRB sources can be considered as standard candles for determining cosmological distance.

8 Thermodynamic of photon-pair sphere formation

It is necessary to study the thermodynamic of photon-pair sphere formation in gravitation collapses. It gives further insight into the dynamics of baryon relaxation (virial theorem) and photon-pair sphere formation in the gravo-thermal dynamics during gravitational collapses. It is very different from the hydrodynamical evolution of the photon-pair sphere.

8.1 Negative pressure and gravitational energy gain

The first thermodynamics law for the adiabatic transformation of the system, in which the particle number changes in time, is given by [70, 71],

$$dQ = d(\varrho V) + \mathcal{P}dV - \frac{\varrho + \mathcal{P}}{\tilde{n}}d(\tilde{n}V), \quad dQ = 0. \quad (8.1)$$

The system is of the volume V , the particle number density \tilde{n} , usual internal energy density ϱ and pressure \mathcal{P} . In Eq. (8.1), the third term of the negative sign represents the system gains energy. It is due to the change in the particle number $\tilde{n}V$. The thermal pressure \mathcal{P} is determined by the energy production $d\varrho$ and particle production $d\tilde{n}$. Equation (8.1) is equivalent to $d\varrho = (\varrho + \mathcal{P})d\tilde{n}/\tilde{n}$ or $\mathcal{P} = (\tilde{n}d\varrho - \varrho d\tilde{n})/d\tilde{n}$.

As the time-scale hierarchy (4.6) discussed in Sec. 4, the macroscopic gravitational collapse and hydrodynamic processes are approximately adiabatic, w.r.t. the microscopic processes for creation and thermalization of particle energy and the number distributions. We apply the thermodynamics law (8.1) to the system that undergoes gravitational collapse and photon-pair sphere formation. The self-gravitating system contains (i) the baryon core of density n and conserved baryon number N ; (ii) the photon-pair sphere of density n_γ and increasing photon number N_γ . The photon production is caused by hadron collisions, consuming the hadron “heat” energy dF (2.3). The total internal energy density $\varrho = F/V + \rho_\gamma$ and pressure $\mathcal{P} = p + p_\gamma$. The photon-pair sphere is opaque, and no heat energy is transferred outside the system $dQ = 0$. Considering the first thermodynamics law in the presence of gravitational potential energy, see for example [72], we generalise the law (8.1) to

$$dQ = d(\varrho V) + \mathcal{P}dV - \frac{\rho_\gamma + p_\gamma}{n_\gamma}d(n_\gamma V) + dU, \quad dQ = 0. \quad (8.2)$$

This is the total energy conservation of the system. The baryon core and photon-pair sphere exchange heat energy. This can be seen by rewriting Eq. (8.2) as

$$-d(\rho V) - pdV - dU = d(\rho_\gamma V) + p_\gamma dV - \frac{\rho_\gamma + p_\gamma}{n_\gamma}d(n_\gamma V). \quad (8.3)$$

The left-handed side indicates the hadron collision energy pumped into the photon-pair sphere. The right-handed side can be effectively rewritten as $d(\rho_\gamma V) + (p_\gamma + p_n)dV$ with a negative pressure p_n defined as

$$p_n \equiv -\frac{\rho_\gamma + p_\gamma}{n_\gamma} \frac{d(n_\gamma V)}{dV} < -(\rho_\gamma + p_\gamma) = -4p_\gamma, \quad (8.4)$$

where photon production leads to $d(n_\gamma V) > 0$ and $dn_\gamma > 0$.

In contrast with the normal positive photon pressure p_γ , negative pressure p_n is in energetic favor of gravitational collapse. The total effective photon pressure $(p_\gamma + p_n) < -3p_\gamma$ is negative. Therefore, the photon-pair sphere creation of increasing photon number density $dn_\gamma > 0$ is energetically favourable in gravitational collapse. It gains energy from the hadron collisional energy, which comes from the gravitational potential energy. This result indicates that the total effective heat function of the photon-pair sphere $h_\gamma^{\text{eff}} \equiv h_\gamma + p_n = \rho_\gamma + p_\gamma + p_n$ can be negative, favouring gravitational collapse rather than positively repelling as usually expected. However, when the total photon number stops increasing $d(n_\gamma V) = 0$, the photon-pair sphere becomes a normal relativistic fluid of positive pressure $p_\gamma = \rho_\gamma/3$, pushing outwardly against gravitational attraction. In this article, we do not consider these photon-pair sphere effects on homologous collapse dynamics since the photon-pair sphere energy density ρ_γ is much smaller than the baryon core energy density.

8.2 Entropy increases in particle relaxation and production

We turn now to the second law of thermodynamics. To evaluate the entropy flow and the entropy production, one starts from the total differential of the entropy \mathcal{S} [70, 71],

$$\mathcal{T}d\mathcal{S} = d(\varrho V) + \mathcal{P}dV - \mu d(\tilde{n}V), \quad (8.5)$$

where \mathcal{T} and $\tilde{n}\mu = \varrho + \mathcal{P} - \mathcal{T}\mathcal{S}/V$ are the temperature and chemical potential respectively. Applying the total differential of entropy (8.5) to the self-gravitating system of the baryon core and photon-pair sphere, we have,

$$TdS + T_\gamma dS_\gamma = d(\rho V) + pdV + d(\rho_\gamma V) + p_\gamma dV - \mu_\gamma d(n_\gamma V), \quad (8.6)$$

where T and S are baryon core temperature and entropy, T_γ and S_γ are photon-pair sphere temperature and entropy. The photon-pair sphere chemical potential μ_γ is

$$\mu_\gamma = n_\gamma^{-1} \left(\rho_\gamma + p_\gamma - T_\gamma S_\gamma / V \right). \quad (8.7)$$

Substituting the first law (8.3) to the total differential of entropy (8.6), we obtain the total entropy increase

$$TdS + T_\gamma dS_\gamma = -dU + \frac{T_\gamma S_\gamma}{n_\gamma V} d(n_\gamma V) > 0, \quad (8.8)$$

since $-dU > 0$ and $d(n_\gamma V) > 0$. Assuming the baryon entropy $TdS = -dU$ purely comes from gravitation energy conversion, we have $dS_\gamma = S_\gamma d(n_\gamma V) / n_\gamma V$. This leads

$S_\gamma \propto n_\gamma V$, namely photon entropy produced is proportional to photon number produced.

We thus conclude that in gravitational collapses, the processes of baryon relaxation and photon-pair sphere formation are energetically and entropically favourable

9 Conclusion and remarks

Using a simplified model describing homologous gravitational collapses of massive and dense stellar baryon cores, we present a preliminary understanding of how and why gravo-thermal catastrophe occurs in gravitational collapses, converting gravitational potential energy to observable photon energy. Such gravo-thermal dynamics attributes to two aspects. (i) From self-gravitating core potential energy, baryons gain their heat energy via collisional relaxation. We adopt the virial theorem to approximately describe this process. (ii) Via baryon collisions, photons are produced and gain their energy from baryons' heat energy. We approximately calculate this process by using the photon production by heavy-ion collisions. The vast difference between macroscopic and microscopic time scales, i.e., the time scale hierarchy (4.6), is *a priori* the prerequisite for using semi-analytical analyses at the qualitative level. The obtained physical results need verifications for theoretical self-consistencies *a posteriori* and compared with observational data. As a result, we show that a photon-pair sphere formation process is energetically and entropically favourable. Such created photon-pair spheres possess fundamental physical quantities, i.e., size, total energy, energy and number densities that possibly qualitatively account for the main energetic features of GRB progenitors. All these quantities uniquely depend on the baryon core centre density $\rho_c(t)$ (7.1), which is determined by homologous core mass M and radius r_s , as well as the eigenvalue (γ, λ_m) of homologous configurations. These configurations represent different GRB sources (events). There are two basic parameters in the baryon core EoS (2.4): the averaged thermal index $1 < \gamma < 4/3$ and maximal core central density $\rho_c^{\max}(\gamma, \kappa) \gtrsim \rho_0$ (5.5). Eliminating the $\rho_c(t)$ -dependence in these physical quantities, we obtain intrinsic correlations (universal scaling laws) among them, in terms of only one parameter $\chi = \chi(\gamma) \sim \mathcal{O}(1)$. These theoretical correlations (scaling laws) and their scaling indices must confront observational data.

In reality, the gravo-thermal dynamics for stellar core collapse and photon-pair sphere formation must be very complex. There are not only violent hadron collisions and photon productions, but also violently strong electromagnetic field fluctuations, plasma oscillations, and hadron-quark phase transition in microscopic scales. As a consequence, the thermal index γ in the effective EoS (2.4) should be a function of space and time. Such γ -inhomogeneity should cause sound velocity (5.4) variation and shock wave occurrence, impacting on homologous collapse and photon-pair sphere formation. Indeed, the macroscopic hydrodynamics of baryon core and photon-pair sphere, on the other hand, play important roles in the gravo-thermal dynamics. Due to the vast time scale hierarchy (4.6), it is very inviting to adopt analytical approaches to microscopic processes and numerical simulation algorithms for macroscopic processes,

to give a quantitative study of the gravo-thermal dynamics in connection with GRB observations.

We end this article by making some remarks on possible relevant issues of neutrino bursts, high-energy photons, cosmic rays and high-frequency gravitation wave emissions. In the photon-pair sphere, the electron-positron pair annihilation $e^+ + e^- \rightarrow \nu + \bar{\nu}$ is the dominant neutrino production, and the neutrino opacity is mainly due to the scattering $\nu + e^\pm \rightarrow \nu + e^\pm$. If neutrinos are trapped inside the photon-pair sphere, the neutrino mean energy $\langle E_\nu \rangle$ is about $T_{e^+e^-} \approx T_\gamma$. At decoupling bursts, neutrino sphere total energy $E_{\text{tot}}^\nu = 3.1 \times 10^{51} \text{erg} [E_{\gamma 52} R_{\gamma 6.5}]^{11/16}$ and mean energy $\langle E_\nu \rangle = 56 \text{ MeV} \times [E_{\gamma 52}]^{1/4} [R_{\gamma 6.5}]^{-3/4}$ [73], where $E_{\gamma 52} = E_\gamma / 10^{52} \text{erg}$ and $R_{\gamma 6.5} = R_\gamma / 10^{6.5} \text{cm}$. They are relevant for observations and should follow the same scaling laws discussed in Sec. 7.2. If neutrinos are not trapped, neutrino continuous emission and cooling processes occur, which may prevent the photon-pair sphere from forming. This does not seem to be the case. The reasons are that (i) electron-positron (e^+e^-) plasma density and size are large enough, see Fig. 5, to trap neutrinos; (ii) the hadronic photon production rate (3.3) is fast enough, namely, its time scale (3.6) is shorter than the time scale (3.7) of e^+e^- pair production. Moreover, due to its weak interaction nature, the $\bar{\nu}\nu$ production time scale is longer than e^+e^- pair production. However, these reasons require a quantitative analysis based on the time scale hierarchy (4.6) and the time scale of photon-pair sphere hydrodynamical expansion. It is worthwhile to mention that in the photon-pair sphere, hot and dense photon-electron-positron plasma modes emit high-frequency ($\omega \sim T_\gamma$) gravitational wave [74, 75].

Last, but certainly not least, we discuss the possibilities for the continuous emissions of ultra-high-energy cosmic rays (protons), ultra-high-energy photons and neutrinos from the photon-pair sphere. Due to the gravitational attraction and hydrodynamical expulsion, the photon-pair sphere is split into two parts. The inner part of the energy $E_\gamma^{\text{in}} \lesssim E_\gamma/2$ falls inward, while its outer part expands outward, and the separatrix radius locates at $R_{\text{sep}} \approx 4GM$ [65]. As mentioned, the expanding outer part leads to complex GRB phenomena. While the falling inner part takes a long time to trap onto the horizon $R_+ = 2GM$ because of the general relativity effect. The inner part energy density $\rho_\gamma \sim T_\gamma^4 > m_e^4$ indicates violent fluctuating electromagnetic fields $\tilde{E}_{\text{em}} > E_c = B_c = m_e^2/e$. These fields possibly accelerate protons to ultra high energies $\mathcal{E} \approx e\tilde{E}_{\text{em}}\ell$, up to GeV, TeV, PeV, EeV and 10^{21} eV, in small lengths $\ell < (\mathcal{E}/m_e)\lambda_e$ and times $\tau < (\mathcal{E}/m_e)\tau_e$, where the Compton length $\lambda_e \sim 10^{-11} \text{cm}$ and time $\tau_e \sim 10^{-21} \text{sec}$. These high-energy protons can be candidates of high-energy cosmic rays. They produce high-energy photons via possible QED processes by interacting with charge particles and external classical magnetic fields. They produce high-energy neutrinos via proton-proton collisions. The inner part size and optical depth are much smaller than the outer part. The inner part activities of releasing particles and energy are continuous, in contrast to the outer part decoupling bursts. It may account for the high-energy cutoff power-law spectrum of GRBs. The inner part activities can be observed after the outer part becomes transparent. All these speculations need further studies.

10 Acknowledgment

The author thanks Professor Ruffini and ICRANet members for many discussions on GRB physics and phenomena.

11 Appendix: the time evolutions of homologous profiles

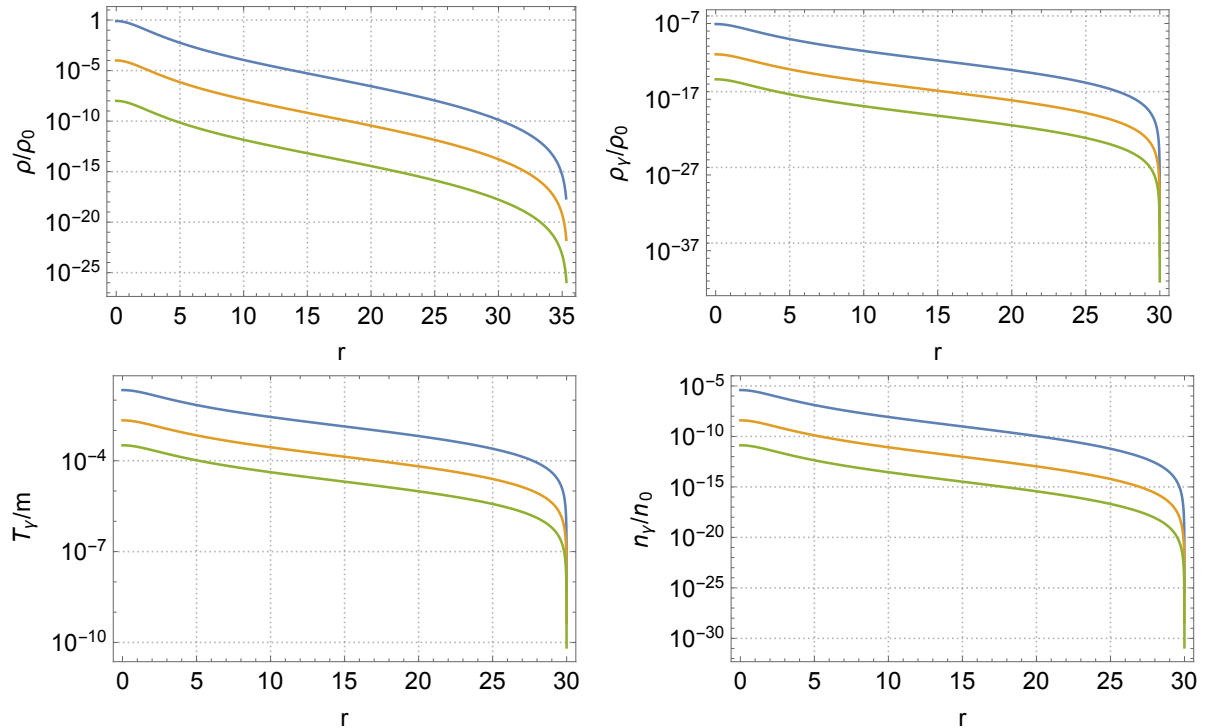


Figure 7. Colours on line. The green (below) line for time $t_1/\tau_{\min} \approx 10^6$, orange (middle) line for time $t_2/\tau_{\min} \approx 10^4$ and blue (above) line for time $t_3/\tau_{\min} \approx 10^2$, see Fig. 2. As described in text, the time sequence $t_1 > t_2 > t_3$ for ongoing gravitational collapses is in the inverse direction of the time arrow, from $t \gg \tau_{\min}$ to $t = \tau_{\min}$. These figures show the time evolutions of homologous profiles of baryon core density, photon-pair sphere temperature, energy and number densities for the eigenvalue $(\gamma, \lambda_m) = (1.23, 8 \times 10^{-5})$. Top panel: the baryon core density $\rho(r, t)/\rho_0$ (5.2) (left), and photon energy density $\rho_\gamma(r, t)/\rho_0$ (6.3) (right). Bottom panel: the photon temperature $\langle T_\gamma(r, t) \rangle/m$ (6.1) (left) and number density $\langle n_\gamma \rangle/n_0$ (6.4) (right). Note that typical baryon mass $m \approx 1$ GeV, the nuclear saturation density $\rho_0 \approx 2.4 \times 10^{35}$ ergs/cm³ and $n_0 \approx 1.6 \times 10^{38}$ /cm³.

For readers' convenience, we show in Fig. 7 the time evolutions of homologous profiles of baryon core density, photon-pair sphere temperature, energy and number densities. These homologous profiles do not change their shapes in time. However, their amplitudes change greatly in time as the gravitational collapse process proceeds. Note that the homologous core radius r_s and photon-pair sphere radius r_γ are independent of the collapsing time t . They depend on the eigenvalue (γ, λ_m) , core centre mass

ρ_c and homologous core mass M , see Eq. (5.13). Moreover, Figure 7 gives us some intuitive ideas about how these homologous profiles smoothly evolving and varying in macroscopic time and length scale. Whereas the microscopic processes of baryon collisional relaxation, photon production and thermalisation violently take place in tiny spacetime shells of width τ_{micro} and $\ell_{\text{micro}} \approx c\tau_{\text{micro}}$.

References

- [1] T. Piran, *The physics of gamma-ray bursts*, *Reviews of Modern Physics* **76** (2004) 1143 [[astro-ph/0405503](#)].
- [2] P. Mészáros, *Gamma-ray bursts*, *Reports on Progress in Physics* **69** (2006) 2259 [[astro-ph/0605208](#)].
- [3] E. Berger, *Short-Duration Gamma-Ray Bursts*, *Annual Review of Astron and Astrophys* **52** (2014) 43 [[1311.2603](#)].
- [4] P. D’Avanzo, *Short gamma-ray bursts: A review*, *Journal of High Energy Astrophysics* **7** (2015) 73.
- [5] P. Kumar and B. Zhang, *The physics of gamma-ray bursts & relativistic jets*, *Physics Reports* **561** (2015) 1 [[1410.0679](#)].
- [6] B. Zhang, *The Physics of Gamma-Ray Bursts*. Cambridge University Press, 2018, [10.1017/9781139226530](#).
- [7] R. Ruffini, R. Moradi, J. A. Rueda, L. Becerra, C. L. Bianco, C. Cherubini et al., *On the gev emission of the type i bdhn grb 130427a*, *The Astrophysical Journal* **886** (2019) 82 [[1812.00354](#)].
- [8] J. A. Rueda, R. Ruffini and Y. Wang, *Induced Gravitational Collapse, Binary-Driven Hypernovae, Long Gamma-ray Bursts and Their Connection with Short Gamma-ray Bursts*, *Universe* **5** (2019) 110 [[1905.06050](#)].
- [9] R. Ruffini, R. Moradi, J. A. Rueda, L. Li, N. Sahakyan, Y. C. Chen et al., *The morphology of the X-ray afterglows and of the jetted GeV emission in long GRBs*, *Monthly Notices of the Royal Astronomical Society* **504** (2021) 5301 [[2103.09142](#)].
- [10] S. E. Woosley, *Gamma-Ray Bursts from Stellar Mass Accretion Disks around Black Holes*, *The Astrophysical Journal* **405** (1993) 273.
- [11] C. L. Fryer and S. E. Woosley, *Helium Star/Black Hole Mergers: A New Gamma-Ray Burst Model*, *The Astrophysical Journal Letters* **502** (1998) L9 [[astro-ph/9804167](#)].
- [12] S. R. Kulkarni, D. A. Frail, M. H. Wieringa, R. D. Ekers, E. M. Sadler, R. M. Wark et al., *Radio emission from the unusual supernova 1998bw and its association with the γ -ray burst of 25 April 1998*, *Nature* **395** (1998) 663.
- [13] A. I. MacFadyen and S. E. Woosley, *Collapsars: Gamma-Ray Bursts and Explosions in “Failed Supernovae”*, *The Astrophysical Journal* **524** (1999) 262 [[astro-ph/9810274](#)].

- [14] G. Preparata, R. Ruffini and S.-S. Xue, *The dyadosphere of black holes and gamma-ray bursts*, *Astron. Astrophys.* **338** (1998) L87 [[astro-ph/9810182](#)].
- [15] G. Preparata, R. Ruffini and S.-S. Xue, *On the dyadosphere of black holes*, *J. Korean Phys. Soc.* **42** (2003) S99 [[astro-ph/0204080](#)].
- [16] R. Ruffini and S.-S. Xue, *Dyadosphere formed in gravitational collapse*, *AIP Conf. Proc.* **1059** (2008) 72 [[0810.1438](#)].
- [17] R. Ruffini, G. Vereshchagin and S.-S. Xue, *Electron-positron pairs in physics and astrophysics: from heavy nuclei to black holes*, *Phys. Rept.* **487** (2010) 1 [[0910.0974](#)].
- [18] W.-B. Han, R. Ruffini and S.-S. Xue, *Electron and positron pair production of compact stars*, *Phys. Rev. D* **86** (2012) 084004 [[1110.0700](#)].
- [19] R. Ruffini and S.-S. Xue, *Gravitational and electric energies in the collapse of a spherical thin-shell capacitor*, *Phys. Lett. A* **377** (2013) 2450 [[1302.5356](#)].
- [20] J. S. Bloom, S. R. Kulkarni and S. G. Djorgovski, *The Observed Offset Distribution of Gamma-Ray Bursts from Their Host Galaxies: A Robust Clue to the Nature of the Progenitors*, *The Astronomical Journal* **123** (2002) 1111 [[astro-ph/0010176](#)].
- [21] P. A. Crowther, *Physical Properties of Wolf-Rayet Stars*, *Annual Review of Astron and Astrophys* **45** (2007) 177 [[astro-ph/0610356](#)].
- [22] S. E. Woosley and A. Heger, *The Progenitor Stars of Gamma-Ray Bursts*, *The Astrophysical Journal* **637** (2006) 914 [[astro-ph/0508175](#)].
- [23] J. P. U. Fynbo, D. Watson, C. C. Thöne, J. Sollerman, J. S. Bloom, T. M. Davis et al., *No supernovae associated with two long-duration γ -ray bursts*, *Nature* **444** (2006) 1047 [[astro-ph/0608313](#)].
- [24] R. Perna, D. Lazzati and B. Giacomazzo, *Short Gamma-Ray Bursts from the Merger of Two Black Holes*, *The Astrophysical Journal Letters* **821** (2016) L18 [[1602.05140](#)].
- [25] Z.-P. Jin, X. Li, H. Wang, Y.-Z. Wang, H.-N. He, Q. Yuan et al., *Short GRBs: Opening Angles, Local Neutron Star Merger Rate, and Off-axis Events for GRB/GW Association*, *The Astrophysical Journal* **857** (2018) 128 [[1708.07008](#)].
- [26] R. Ruffini, J. D. Salmonson, J. R. Wilson and S. S. Xue, *On the pair-electromagnetic pulse from an electromagnetic black hole surrounded by a baryonic remnant*, *Astronomy and Astrophysics* **359** (2000) 855 [[astro-ph/0004257](#)].
- [27] P. Mészáros and M. J. Rees, *Collapsar Jets, Bubbles, and Fe Lines*, *The Astrophysical Journal Letters* **556** (2001) L37 [[astro-ph/0104402](#)].
- [28] A. de Rújula, *GRBs in the cannonball model: an overview*, in *New Views on Microquasars*, P. Durouchoux, Y. Fuchs and J. Rodriguez, eds., p. 185, Jan., 2003, [astro-ph/0207033](#).

- [29] Y. Wang, Y.-Z. Fan and D.-M. Wei, *Are GRB 090423 and Similar Bursts due to Superconducting Cosmic Strings?*, *Physical Review Letters* **106** (2011) 259001 [[1105.5147](#)].
- [30] D. Nakauchi, K. Kashiyama, Y. Suwa and T. Nakamura, *Blue Supergiant Model for Ultra-long Gamma-Ray Burst with Superluminous-supernova-like Bump*, *The Astrophysical Journal* **778** (2013) 67 [[1307.5061](#)].
- [31] C. L. Fryer, J. A. Rueda and R. Ruffini, *Hypercritical Accretion, Induced Gravitational Collapse, and Binary-Driven Hypernovae*, *The Astrophysical Journal Letters* **793** (2014) L36 [[1409.1473](#)].
- [32] R. Ruffini, J. A. Rueda, M. Muccino, Y. Aimuratov, L. M. Becerra, C. L. Bianco et al., *On the Classification of GRBs and Their Occurrence Rates*, *The Astrophysical Journal* **832** (2016) 136 [[1602.02732](#)].
- [33] T. Hayakawa and K. Maeda, *A Collapsar Model with Disk Wind: Implications for Supernovae Associated with Gamma-Ray Bursts*, *The Astrophysical Journal* **854** (2018) 43 [[1801.09681](#)].
- [34] L. Li, X.-F. Wu, W.-H. Lei, Z.-G. Dai, E.-W. Liang and F. Ryde, *Constraining the type of central engine of grbs with swift data*, *Astrophys. J. Suppl.* **236** (2018) 26 [[1712.09390](#)].
- [35] D. Lynden-Bell, *Statistical mechanics of violent relaxation in stellar systems*, *Mon. Not. Roy. Astron. Soc.* **136** (1967) 101.
- [36] D. Lynden-Bell and R. Wood, *The gravo-thermal catastrophe in isothermal spheres and the onset of red-giant structure for stellar systems*, *Monthly Notices of the Royal Astronomical Society* **138** (1968) 495.
- [37] T. Padmanabhan, *Antonov instability and gravothermal catastrophe—revisited*, *The Astrophysical Journal Supplement Series* **71** (1989) 651.
- [38] P. H. Chavanis, *Gravitational instability of finite isothermal spheres in general relativity. analogy with neutron stars*, *Astronomy and Astrophysics* **381** (2002) 709 [[astro-ph/0108230](#)].
- [39] P. H. Chavanis, *Gravitational instability of isothermal and polytropic spheres*, *Astronomy and Astrophysics* **401** (2003) 15 [[astro-ph/0207080](#)].
- [40] M. C. Sormani and G. Bertin, *Gravothermal catastrophe: The dynamical stability of a fluid model*, *Astronomy and Astrophysics* **552** (2013) A37 [[1301.6038](#)].
- [41] Z. Roupas, *Relativistic gravothermal instabilities*, *Class. Quant. Grav.* **32** (2015) 135023 [[1411.4267](#)].
- [42] Z. Roupas, B. Kocsis and S. Tremaine, *Isotropic-nematic phase transitions in gravitational systems*, *The Astrophysical Journal* **842** (2017) 90 [[1701.03271](#)].

- [43] Á. Takács and B. Kocsis, *Isotropic-nematic phase transitions in gravitational systems. ii. higher order multipoles*, *The Astrophysical Journal* **856** (2018) 113 [[1712.04449](#)].
- [44] P. Dutta and P. K. Karmakar, *Dynamics of gravoviscothermal instability in complex astrofluids amid cosmic radiative moderation effects*, *Astrophysics and Space Science* **364** (2019) 217.
- [45] S. Turbide, R. Rapp and C. Gale, *Hadronic production of thermal photons*, *Phys. Rev. C* **69** (2004) 014903 [[hep-ph/0308085](#)].
- [46] J. I. Kapusta, P. Lichard and D. Seibert, *High-energy photons from quark - gluon plasma versus hot hadronic gas*, *Phys. Rev. D* **44** (1991) 2774.
- [47] J. I. Kapusta, P. Lichard and D. Seibert, *High-energy photons from quark - gluon plasma versus hot hadronic gas*, *Nucl. Phys. A* **544** (1992) 485C.
- [48] P. B. Arnold, G. D. Moore and L. G. Yaffe, *Photon emission from quark gluon plasma: Complete leading order results*, *JHEP* **12** (2001) 009 [[hep-ph/0111107](#)].
- [49] C. Gale, Y. Hidaka, S. Jeon, S. Lin, J.-F. Paquet, R. D. Pisarski et al., *Production and elliptic flow of dileptons and photons in a matrix model of the quark-gluon plasma*, *Phys. Rev. Lett.* **114** (2015) 072301 [[1409.4778](#)].
- [50] Y. Hidaka, S. Lin, R. D. Pisarski and D. Satow, *Dilepton and photon production in the presence of a nontrivial polyakov loop*, *JHEP* **10** (2015) 005 [[1504.01770](#)].
- [51] P. Goldreich and S. V. Weber, *Homologously collapsing stellar cores*, *Astrophysical Journal* **238** (1980) 991.
- [52] G. Vujanovic, C. Young, B. Schenke, R. Rapp, S. Jeon and C. Gale, *Dilepton emission in high-energy heavy-ion collisions with viscous hydrodynamics*, *Phys. Rev. C* **89** (2014) 034904 [[1312.0676](#)].
- [53] J. K. Daugherty and I. Lerche, *On pair production in intense electromagnetic fields occurring in astrophysical situations*, *Astrophys. and Space Sci.* **38** (1975) 437.
- [54] J. K. Daugherty and A. K. Harding, *Pair production in superstrong magnetic fields.*, *Astrophysical Journal* **273** (1983) 761.
- [55] K. A. van Riper and J. M. Lattimer, *Stellar core collapse. i - infall epoch*, *Astrophys. J.* **249** (1981) 270.
- [56] Y. Cao and Y.-Q. Lou, *Perturbation analysis of a general polytropic homologously collapsing stellar core*, *Monthly Notices of the Royal Astronomical Society* **400** (2009) 2032 [[0908.3225](#)].
- [57] Y.-Q. Lou and B. Lian, *Three-dimensional hydrodynamic instabilities in stellar core collapses*, *Monthly Notices of the Royal Astronomical Society* (2012) [[1111.2935](#)].
- [58] D. Lynden-Bell, *Homology in the evolution of cluster cores, cores, in dynamics of stellar systems*, *Proceedings from IAU Symposium no. 69, A. Hayli ed., Besancon, France, 9–13 September 1974.* **69** (1974) 27.

- [59] S. L. Shapiro, *The dissolution of globular clusters containing massive black holes.*, *Astrophysical Journal* **217** (1977) 281.
- [60] P. Bedaque and A. W. Steiner, *Sound velocity bound and neutron stars*, *Phys. Rev. Lett.* **114** (2015) 031103 [[1408.5116](#)].
- [61] R. Ruffini, L. Vitagliano and S. S. Xue, *On plasma oscillations in strong electric fields*, *Phys.Lett. B559 (2003) 12-19* (2003) [[astro-ph/0302549](#)].
- [62] J. Ehlers, *General relativity and kinetic theory in general relativity and cosmology, Proceedings of cours 47 of the International School of Physics: Enrico Fermi, ed. Sachs, R.K. , Academic Press, New York. (1971) .*
- [63] R. Ruffini, J. D. Salmonson, J. R. Wilson and S.-S. Xue, *On the pair electromagnetic pulse of a black hole with electromagnetic structure*, *Astron. Astrophys.* **350** (1999) 334 [[astro-ph/9907030](#)].
- [64] R. Ruffini, J. D. Salmonson, J. R. Wilson and S.-S. Xue, *On the pair-electromagnetic pulse from an electromagnetic black hole surrounded by a baryonic remnant*, *Astron. Astrophys.* **359** (2000) 855 [[astro-ph/0004257](#)].
- [65] R. Ruffini, L. Vitagliano and S.-S. Xue, *On a separatrix in the gravitational collapse to an overcritical electromagnetic black hole*, *Phys. Lett. B* **573** (2003) 33 [[astro-ph/0309022](#)].
- [66] L. Amati, F. Frontera, M. Tavani, J. J. M. in't Zand, A. Antonelli, E. Costa et al., *Intrinsic spectra and energetics of beposax gamma-ray bursts with known redshifts*, *Astronomy & Astrophysics* **390** (2002) 81 [[astro-ph/0205230](#)].
- [67] D. Yonetoku, T. Murakami, T. Nakamura, R. Yamazaki, A. K. Inoue and K. Ioka, *Gamma-ray burst formation rates inferred from the spectral peak energy-peak luminosity relation*, *Astrophys. J.* **609** (2004) 935 [[astro-ph/0309217](#)].
- [68] P. Mészáros and M. J. Rees, *Steep slopes and preferred breaks in gamma-ray burst spectra: The role of photospheres and comptonization*, *The Astrophysical Journal* **530** (2000) 292 [[astro-ph/9908126](#)].
- [69] B. Zhang, Y. Wang and L. Li, *Dissecting the energy budget of a gamma-ray burst fireball*, *Astrophys. J. Lett.* **909** (2021) L3 [[2102.04968](#)].
- [70] I. Prigogine, J. Gehehiau, E. Gunzig and P. Nardone, *Thermodynamics of cosmological matter creation*, *Proceedings of the National Academy of Science* **85** (1988) 7428.
- [71] I. Prigogine, J. Gehehiau, E. Gunzig and P. Nardone, *Thermodynamics and cosmology*, *General Relativity and Gravitation* **21** (1989) 767.
- [72] F. O. Koenig, *Note on thermodynamic equilibrium in the gravitational field*, *J. Phys. Chem.* **40** (1936) 373.
- [73] H. B. J. Koers and R. A. M. J. Wijers, *The effect of neutrinos on the initial fireballs in gamma-ray bursts*, *Mon. Not. Roy. Astron. Soc.* **364** (2005) 934 [[astro-ph/0505533](#)].

- [74] S. Weinberg, *Gravitation and Cosmology: Principles and Applications of the General Theory of Relativity*. 1972.
- [75] W.-B. Han and S.-S. Xue, *Electromagnetic and gravitational radiation from the coherent oscillation of electron-positron pairs and fields*, *Phys. Rev. D* **89** (2014) 024008 [[1307.6148](#)].